

Estimating scale-specific and localized spatial patterns in allele frequency

Jesse R. Lasky^{1,2}, Margarita Takou¹, Diana Gamba¹, and Timothy H. Keitt³

¹Department of Biology, Pennsylvania State University, University Park, PA 16802, USA

²Correspondence: lasky@psu.edu

³Department of Integrative Biology, University of Texas at Austin, Austin, TX 78712, USA

May 4, 2024

Abstract

Characterizing spatial patterns in allele frequencies is fundamental to evolutionary biology because these patterns contain evidence of underlying processes. However, the spatial scales at which gene flow, changing selection, and drift act are often unknown. Many of these processes can operate inconsistently across space, causing non-stationary patterns. We present a wavelet approach to characterize spatial pattern in allele frequency that helps solve these problems. We show how our approach can characterize spatial patterns in relatedness at multiple spatial scales, i.e. a multi-locus wavelet genetic dissimilarity. We also develop wavelet tests of spatial differentiation in allele frequency and quantitative trait loci (QTL). With simulation we illustrate these methods under different scenarios. We also apply our approach to natural populations of *Arabidopsis thaliana* to characterize population structure and identify locally-adapted loci across scales. We find, for example, that *Arabidopsis* flowering time QTL show significantly elevated genetic differentiation at 300 to 1300 km scales. Wavelet transforms of allele frequencies offer a flexible way to reveal geographic patterns and underlying evolutionary processes.

Running head: Wavelet-transformed spatial genetic patterns

Keywords: Landscape genetics, F_{ST} , local adaptation, isolation by distance

1 Introduction

2 Geographic clines in allele frequency are a classic pattern in evolutionary biology, being frequently observed in nature and having extensive theory for the
3 underlying processes. For example, theory describes how limited gene flow and drift (Wright 1931) or changing selection (Haldane 1948) can generate allele frequency differences between populations. Accordingly, researchers often estimate and model spatial allele frequency patterns to make inferences about underlying evolutionary and ecological mechanisms. To do so, researchers often divide sampled individuals into discrete groups (populations) among which differences in allele frequencies are calculated. A common such approach involves estimating F_{ST} , the proportion of total allele frequency variation that differs between discrete populations (Lewontin and Krakauer 1973; Wright 1949).

13 However, many species exist as more or less continuously distributed populations. Theoretical study of allele frequency change across continuous populations began as early as Wright (1943) and Malécot (1948), who found expectations for genetic differentiation or kinship as functions of gene flow and geographic distance. Later progress included diffusion models (Nagylaki 1978) and stepping stone/lattice models (Kimura and Weiss 1964) giving expectations for correlation in allele frequencies across distance, and models accounting for population regulation by negative density dependence (Nick H. Barton, Depaulis, and Etheridge 2002).

22 Despite these theoretical advances, the statistical tools for inference on continuously distributed populations have lagged (Bradburd and Peter L. Ralph 2019; Hancock, Toczydlowski, and Bradburd 2023). Nevertheless, statistical approaches to studying spatial pattern in continuous populations include models relating landscape features to gene flow (McRae et al. 2008), calculating correlations between spatial functions and genotype (Wagner, Chávez-Pesqueira, and Forester 2017; Yang et al. 2012), and applying discrete landscape grids to identify geographic regions where genetic turnover is particularly high or low (Petkova, Novembre, and Stephens 2016). Approaches have been developed to estimate the average distance of gene flow from the slope of genetic divergence versus geographic distance (Rousset 2000; X. Vekemans and O. J. Hardy 2004), to estimate localized genetic "neighborhoods" (Shirk and Cushman 2014; Wright 1946), and to model both discrete and continuous relatedness patterns simultaneously (Bradburd, G. M. Coop, and Peter L. Ralph 2018).

36 In recent years researchers have collected many large, broadly distributed DNA sequence datasets from diverse species (Alonso-Blanco et al. 2016; Machado et al. 2021; J. Wang et al. 2020; Yeaman et al. 2016). Statistical inference can be applied to these data to understand gene flow, demographic histories, and spatially-varying selection. Despite the progress made by previous approaches, there remain challenges.

42 **1.1 The form and scale of relevant spatial patterns is un-**
 43 **known**

44 Humans can infer seemingly meaningful patterns in even randomly generated
 45 images (Ayton and Fischer 2004; Blakemore et al. 2003; Fyfe et al. 2008). So
 46 what are the spatial patterns we are looking for? The functional forms (i.e.
 47 shapes) of both spatially-varying selection and neutral processes (e.g. dispersal
 48 kernels) are often unknown, as are the forms of resulting spatial patterns. For
 49 example, the specific environmental gradients driving changing selection are
 50 often not known, nor is the spatial scale at which they act, and whether they
 51 change at the same rate consistently across a landscape.

52 In the case of neutral processes, a homogeneous landscape approximately
 53 at equilibrium is rarely of interest to empiricists. Instead, the influence of het-
 54 erogeneous landscapes (Manel et al. 2003) and historical contingency is usually
 55 a major force behind spatial patterns in allele frequency and traits (Excoffier
 56 and Ray 2008). As a result, researchers often attempt to characterize spatial
 57 patterns of relatedness and genetic similarity to make inferences about varia-
 58 tion in gene flow (McRae et al. 2008; Peterman 2018; I. J. Wang, Savage, and
 59 Bradley Shaffer 2009) and recent population expansion (Slatkin 1993). The in-
 60 fluence of gene flow, drift, and range expansion can occur at a variety of spatial
 61 scales, and in different ways across a heterogenous landscape. For example, the
 62 rate at which relatedness decays over geographic distance can change abruptly
 63 at major barriers (Rosenberg et al. 2005). However, the scale-specificity and
 64 non-stationarity of such patterns can be challenging to characterize.

65 **1.2 The spatially-varying selective gradients causing local**
 66 **adaptation are unknown**

67 One important force behind allele frequency clines is changing selection due
 68 to environmental gradients, resulting in local adaptation. However, it is often
 69 not clear what environmental gradients drive local adaptation (Kawecki and
 70 Ebert 2004). This is especially true of non-model systems and those with little
 71 existing natural history knowledge. Even for well-studied species, it is not trivial
 72 to identify the specific environmental conditions that change in space and drive
 73 local adaptation. Ecology is complex, and abiotic and biotic conditions are high-
 74 dimensional. Rather than *a priori* selection of a putative selective gradient,
 75 an alternative approach is to search for spatial patterns in allele frequencies
 76 that cannot be explained by neutral processes. This approach is embodied
 77 by several statistics and approaches, such as F_{ST} (Weir and Cockerham 1984),
 78 XtX (Gautier 2015), spatial ancestry analysis (SPA) (Yang et al. 2012), Moran's
 79 eigenvector maps (MEMs) (Wagner, Chávez-Pesqueira, and Forester 2017), and
 80 others.

81 1.3 Many approaches rely on discretization of population 82 boundaries

83 Some of the aforementioned approaches rely on dividing sampled individuals
84 into discrete spatial groups. F_{ST} is one such approach, that was introduced by
85 Wright (1949) and defined as the "correlation between random gametes, drawn
86 from the same subpopulation, relative to the total", where the definition of "total"
87 has been interpreted differently by different authors (Bhatia et al. 2013).
88 The classic approach of calculating F_{ST} to test for selection was usually applied
89 to a small number of locations, a situation when discretization (i.e. deciding
90 which individuals genotyped belong in which population) was a simpler problem.
91 Current studies often sample and sequence individuals from hundreds of
92 locations, and so the best approach for discretizing these genotyped individuals
93 into defined 'populations' is less clear. In addition to the spatial scale of
94 subpopulations, at issue is precisely where to place the boundaries between pop-
95 ulations. The problem is enhanced for broadly distributed species, connected by
96 gene flow, that lack clear spatially distinct populations (Emily B. Josephs et al.
97 2019). Even if clustering algorithms appear to show clustering of genotypes,
98 these methods can be sensitive to sampling bias (e.g. geographic clustering)
99 and can mislead as to the existence of discrete subpopulations (Frantz et al.
100 2009; Serre and Pääbo 2004).

101 Some approaches are not limited by discretization, and might be gener-
102 ally termed "population-agnostic" because discrete populations are not defined.
103 These instead use ordination of genetic loci or geographic location. Approaches
104 that use ordination (such as PCA) of genetic loci look for particular loci with
105 strong loadings on PCs (Duforet-Frebbourg et al. 2016) or traits with an unex-
106 pectedly high correlation with individual PCs (Emily B. Josephs et al. 2019).
107 Alternatively, ordination of distance or spatial neighborhood matrices can create
108 spatial functions that can be used in correlation tests with genetic loci (Wagner,
109 Chávez-Pesqueira, and Forester 2017). However, ordinations to create individ-
110 ual rotated axes are not done with respect to biology and so might not be ideal
111 for characterizing biological patterns. For example, ordinations of genetic loci
112 are heavily influenced by global outliers of genetic divergence (Peter, Petkova,
113 and Novembre 2020) and uneven sampling (McVean 2009). Ordinations like
114 PCA also often lack parametric null distributions for hypothesis testing.

115 1.4 Wavelet characterization of spatial pattern

116 Instead of discretizing sampled locations into populations, one could model allele
117 frequencies with flexible but smooth functions. Wavelet transforms allow one
118 to characterize the location and the scale or frequency of a signal (Daubechies
119 1992). Daubechies (1992) gives a nice analogy of wavelet transforms: they
120 are akin to written music, which indicates a signal of a particular frequency
121 (musical notes of different pitch) at a particular location (the time at which
122 the note is played, in the case of music). Applying this analogy to genetics, the
123 frequency is the rate at which allele frequencies change in space, and the location

is the part of a landscape where allele frequencies change at this rate. Applying wavelet basis functions to spatial genetic data could allow us to characterize localized patterns in allele frequency, and dilating the scale of these functions could allow us to characterize scale-specific patterns in allele frequency (see Figure S1 in File S1 for an example). Note that wavelets are distinct from Fourier analysis. Wavelets capture localized signals because the basis functions' variance goes to zero moving away from the focal location, while Fourier can only capture global average patterns as it uses stationary (unchanging) basis functions. Wavelet transforms have had some recent applications in modeling ancestry along the genome (Groh and G. Coop 2023; Pugach et al. 2011) but have not been implemented to model geographic genetic patterns.

Keitt (2007) created a wavelet approach for characterizing spatial patterns in ecological communities. He used this approach to identify locations and scales with particular high community turnover, and created null-hypothesis testing of these patterns. These spatial patterns in the abundance of multiple species are closely analogous to spatial patterns in allele frequency of many genetic markers across the genome, and previous spatial genetic studies have also profited by borrowing tools from spatial community ecology (Fitzpatrick and Keller 2015; Jesse R. Lasky, Des Marais, et al. 2012). Here we modify and build on this approach to characterize spatial pattern in allele frequency across the genome and at individual loci.

2 Methods

2.1 Wavelet characterization of spatial pattern in allele frequency

Our implementation here begins by following the work of Keitt (2007) in characterizing spatial community turnover, except that we characterize genomic patterns using allele frequencies of multiple loci in place of abundances of multiple species in ecological communities. In later sections of this paper we build off this approach and develop new tests for selection on specific loci. Our implementation of wavelets allows estimation of scale-specific signals (here, allele frequency clines) centered on a given point, a, b , in two-dimensional space. We use a version of the Difference-of-Gaussians (DoG) wavelet function (Figure S1 in File S1) (Muraki 1995). We start with a Gaussian smoothing function centered at a, b for a set of sampling points $\Omega = \{(u_1, v_1), (u_2, v_2), \dots, (u_n, v_n)\}$, which takes the form

$$\eta_{a,b}^s(x, y) = \frac{k\left(\frac{x-a}{s}, \frac{y-b}{s}\right)}{\sum_{(u,v) \in \Omega} k\left(\frac{u-a}{s}, \frac{v-b}{s}\right)}, \quad (1)$$

where s controls the scale of analysis and $k(x, y)$ is the Gaussian kernel $k(x, y) = e^{-(x^2+y^2)/2}$.

The DoG wavelet function then takes the form

$$_{a,b}^s(x,y) = \eta_{a,b}^s(x,y) - \eta_{a,b}^{\beta s}(x,y) \quad (2)$$

162 where $\beta > 1$, and so the larger scale smooth function is subtracted from
 163 the smaller scale smooth to characterize the scale-specific pattern. If we use
 164 $\beta = 1.87$, then the dominant scale of analysis resulting from the DoG is s
 165 distance units (Keitt 2007). This formulation of the wavelet kernel is similar in
 166 shape to the derivative-of-Gaussian kernel and has the advantage of maintaining
 167 admissibility (Daubechies 1992) even near boundaries, as each of the smoothing
 168 kernels $\eta_{a,b}^s$ are normalized over the samples such that their difference integrates
 169 to zero.

170 Let $f_i(u,v)$ be the major allele frequency of the i th locus from a set of
 171 I biallelic markers at a location with spatial coordinates u,v . The adaptive
 172 wavelet transform of allele frequency data at locus i , centered at a,b and at
 173 scale s is then

$$(T^{wav} f_i)(a,b,s) = \frac{1}{h_{a,b}(s)} \sum_{(u,v) \in \Omega} \psi_{a,b}^s(u,v) f_i(u,v), \quad (3)$$

174 where the right summation is of the product of the smooth function and
 175 the allele frequencies across locations. The magnitude of this summation will
 176 be greatest when the DoG wavelet filter matches the allele frequency cline.
 177 That is, when the shape of the wavelet filter matches the allele frequency cline
 178 in space, the product of $\psi_{a,b}^s(u,v)$ and $f_i(u,v)$ will resonate (increase in ampli-
 179 tude) yielding greater variation among locations in $(T^{wav} f_i)(a,b,s)$, the wavelet-
 180 transformed allele frequencies. When the spatial pattern in the wavelet filter
 181 and allele frequencies are discordant, the variation in their product, and hence
 182 the wavelet-transformed allele frequency, is reduced. For consistency, here we
 183 choose major allele frequency for $f_i(u,v)$, though in practice the signing of alleles
 184 has little impact on our results.

185 The $h_{a,b}(s)$ term in equation 3 is used to normalize the variation in the
 186 wavelet function so that the wavelet transforms $T^{wav} f_i$ are comparable for dif-
 187 ferent scales s and locations a,b :

$$h_{a,b}(s) = \sqrt{\sum_{(u,v) \in \Omega} [\psi_{a,b}^s(u,v)]^2} \quad (4)$$

188 . When a,b is far from locations in Ω relative to the scale s , the Gaussian
 189 functions $[\eta_{a,b}^s(x,y)]$ that make up the wavelet function ψ are only evaluated
 190 over a range where they remain close to zero. Thus unsampled geographic
 191 regions will have very small $h_{a,b}(s)$, the term used to normalize for local variation
 192 in the wavelet basis functions. In turn, very small $h_{a,b}(s)$ dramatically and
 193 undesirably inflates the wavelet transformed allele frequencies (equation 3) in
 194 these geographic regions where there is little sampling relative to s . For this
 195 reason we do not calculate the wavelet transform for locations a,b where there
 196 are no locations sampled closer than $2s$ distance units.

197 Below we illustrate how to apply this wavelet transform (equation 3) of
 198 spatial allele frequency patterns to characterize genome-wide patterns, as well
 199 as to test for local adaption at individual loci.

200 **2.1.1 Wavelet characterization of spatial pattern in multiple loci**

201 Researchers are often interested in characterizing spatial patterns aggregated
 202 across multiple loci across the genome to understand patterns of relatedness,
 203 population structure, and demographic history. Here, we specifically want to
 204 characterize heterogeneity in spatial patterns, because this heterogeneity in pat-
 205 tern may reflect heterogeneity in underlying processes: where there is hetero-
 206 geneity in migration rates, such as where there are migration barriers (Petkova,
 207 Novembre, and Stephens 2016), or where there are recent range expansions such
 208 that spatial patterns are farther from equilibrium (Slatkin 1993).

209 We use

$$D_{a,b}^{wav}(s) = \sqrt{\sum_{i=1}^I [(T^{wav} f_i)(a, b, s)]^2} \quad (5)$$

210 to calculate a "wavelet genetic distance" or "wavelet genetic dissimilarity."
 211 This wavelet genetic dissimilarity is computed as the euclidean distance (in the
 212 space of allele frequencies across the genome) between the genetic composition
 213 centered at a, b and other locations across s distance units. This wavelet genetic
 214 dissimilarity $D_{a,b}^{wav}(s)$ is localized in space and scale-specific. This quantity cap-
 215 tures the level of genetic turnover at scale s centered at a, b , and is capturing
 216 similar information as the increase in average genetic distance between a geno-
 217 type at a, b and other genotypes s distance units away. To obtain the average
 218 dissimilarity across the landscape, one can also calculate the mean of $D_{a,b}^{wav}(s)$
 219 across locations a, b at each sampled site, to get a mean wavelet genetic dissim-
 220 ilarity for s . A benefit of using the wavelet transformation over sliding window
 221 approaches (e.g. Bishop, Chambers, and I. J. Wang 2023) is that wavelets
 222 smoothly incorporate patterns from samples that are not precisely s distance
 223 units away and can be centered at any location of the analyst's choosing.

224 **2.1.2 Testing the null hypothesis of no spatial pattern in allele fre-
 225 quency**

226 A null hypothesis of no spatial pattern in allele frequencies can be generated
 227 by permuting the location of sampled populations among each other. Most
 228 empirical systems are not panmictic, and so this null model is trivial in a sense.
 229 However, comparison with this null across scales and locations can reveal when
 230 systems shift from small-scale homogeneity (from local gene flow) to larger scale
 231 heterogeneity (from limited gene flow) (Keitt 2007).

232 **2.1.3 Simulated neutral patterns across a continuous landscape**

233 To demonstrate the wavelet transformation of allele frequencies, and wavelet
 234 genetic dissimilarity function, we applied these tools to several simulated sce-
 235 narios. First, we conducted forward landscape genetic simulations under neu-
 236 trality using the SLiM software (Haller and Messer 2019), building off published
 237 approaches (C J Battey, Peter L Ralph, and Kern 2020). We simulated out-
 238 crossing, iteroparous, hermaphroditic organisms, with modest lifespans (aver-
 239 age of ~ 4 time steps). Individual fecundity was Poisson distributed, mating
 240 probability (determining paternity) was determined based on a Gaussian kernel
 241 (truncated at three standard deviations), and dispersal distance from mother
 242 was also Gaussian (C. Battey, Peter L Ralph, and Kern 2020). Individuals
 243 became mature in the time step following their dispersal. These parameters
 244 roughly approximate a short lived perennial plant with gene flow via pollen
 245 movement and seed dispersal. Competition reduced survival and decayed with
 246 distance following a Gaussian (truncated at three standard deviations, C J Bat-
 247 tey, Peter L Ralph, and Kern 2020). Near landscape boundaries, survival was
 248 reduced to compensate for lower competition from beyond the landscape mar-
 249 gin (C J Battey, Peter L Ralph, and Kern 2020). Code is available at GitHub
 250 (<https://github.com/jesserlasky/WaveletSpatialGenetic>).

251 We began by characterizing a simple scenario across a continuous land-
 252 scape. We simulated a square two dimensional landscape measuring 25 units
 253 on each side. The standard deviation of mating and dispersal distance σ were
 254 both 0.2, yielding a combined standard deviation of gene flow distances of 0.24
 255 [$(3\sigma^2/2)^{1/2}$]. In this first simulation there was no selection. The population was
 256 allowed to evolve for 100,000 time steps before we randomly sampled 200 indi-
 257 viduals and 1,000 SNPs with a minor allele frequency of at least 0.05. The first
 258 two principal components (PCs) of these SNPs show smooth population struc-
 259 ture across the landscape, and that these two PCs predict the spatial location
 260 of each sample (Figure S2 in File S1).

261 To facilitate interpretation of wavelet transformed allele frequencies
 262 ($T^{wav} f_i(a, b, s)$) we provide two example loci i with distinct spatial patterns
 263 (Figure 1). The first locus has the greatest variance in wavelet transformed
 264 allele frequencies among sampled loci at $s = 0.4$ (Figure 1A-C) while the second
 265 locus has the greatest variance at $s = 12.2$ (Figure 1D-F).

266 We then calculated wavelet dissimilarity $D_{a,b}^{wav}(s)$, aggregating the signals
 267 in $(T^{wav} f_i)(a, b, s)$ across loci i , for each sampled location at a range of spatial
 268 scales s . Here and below we use a set of scales increasing by a constant log
 269 distance interval, as genetic distances are often linearly correlated to log geographic
 270 distances in two dimensions (F. Rousset 1997). The mean across sampled lo-
 271 cations for each scale was calculated and compared to the null distribution for
 272 that scale (Figure S2 in File S1). The null was generated by permuting locations
 273 of sampled individuals as described above, and observed mean of dissimilarity
 274 was considered significant if it was below the 2.5 percentile or above the 97.5
 275 percentile of dissimilarity from null permutations.

276 When comparing our simulated data to the null, we found that mean wavelet

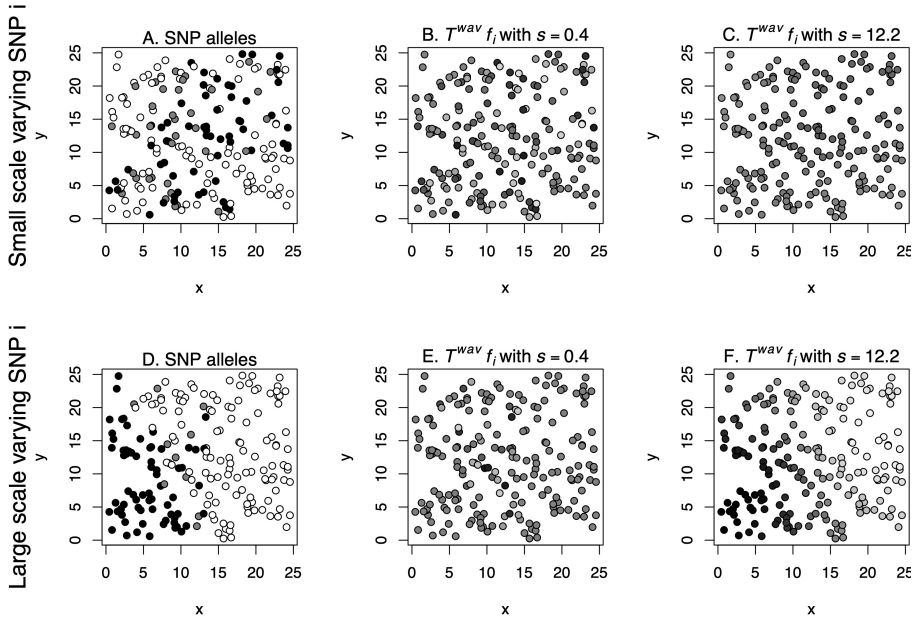


Figure 1: Two example SNPs (rows) with distinct spatial patterns. Shading shows either allelic variation (untransformed, A, D) or variation in wavelet transformed allele frequencies ($T^{wav} f_i(a, b, s)$) (B,C,E,F). The first locus (A-C) has the greatest variance in wavelet transformed allele frequency among sampled loci at $s = 0.4$. The second locus (D-F) has the greatest variance in wavelet transformed allele frequency at $s = 12.2$. For the SNP in the top row, the variance among locations in $(T^{wav} f_i)(a, b, s)$ for $s = 0.4$ is 0.56 (visualized as shading in B), while it is only 0.17 for the SNP in the bottom row (E). For the SNP in the bottom row, the variance among locations in $(T^{wav} f_i)(a, b, s)$ for $s = 12.2$ is 44.46 (visualized as shading in F), while it is only 1.24 for the SNP in the top row (C).

277 genetic dissimilarity was significantly less than expected under the null model
 278 at scales $s \leq 0.93$, due to local homogenization by gene flow (standard deviation
 279 = 0.24). At scales $s \geq 1.24$, wavelet dissimilarity was significantly greater than
 280 expected, due to isolation by distance, with monotonically increasing wavelet
 281 genetic dissimilarity at greater scales (Figure S2 in File S1).

282 To demonstrate how the scale of gene flow influences the wavelet dissimilarity
 283 $D_{a,b}^{wav}(s)$, we also conducted identical simulations as described above but instead
 284 with standard deviations of mating and dispersal distances, σ , of 0.5, 1, 2, or 5,
 285 yielding combined standard deviations of gene flow distances of 0.61, 1.22, 2.45,
 286 and 6.12.

287 To verify that simulations were generating results consistent with theoretical
 288 expectations of continuous populations at equilibrium, we compared the sim-
 289 ulated gene flow parameters with estimations from the simulated data based
 290 on theory. The slope of genetic differentiation versus geographic distance in
 291 two dimensions is expected to be proportional to the inverse of Wright's neigh-
 292 borhood size, $4\pi D\sigma^2$, where D is the effective population density and σ is the
 293 standard deviation of gene flow (Rousset 2000; X. Vekemans and O. J. Hardy
 294 2004; Wright 1943, 1946).

295 We estimated D using $N_e = (4N - 2)/(V + 2)$ where N is census population
 296 size and V is variance in lifetime reproductive output (Kimura and Crow 1963).
 297 We calculated V using the lifetime reproductive output of the individuals dying
 298 in the last 50 time steps. We then divided the estimated N_e by landscape
 299 area (assuming evenly distribution across the landscape) to get effective density
 300 D (X. Vekemans and O. J. Hardy 2004). We used three different genetic
 301 differentiation or kinship metrics (Loiselle et al. 1995; Ritland 1996; Rousset
 302 2000) combined with estimated D to estimate gene flow across a range of true
 303 gene flow parameters (using SPAGeDi v1.5 software, Olivier J. Hardy and Xavier
 304 Vekemans (2002)). We also compared individual pairwise estimates of genetic
 305 differentiation across distance with the theoretically expected slope. Simulations
 306 were run for 100,000 time steps with parameters as described above.

307 We found that the gene flow estimated using the slope of genetic versus
 308 geographic distance and D was closely matched by the simulation parameter
 309 value, especially for the Rousset (2000) genetic differentiation estimator (Figures
 310 S3 and S4 in File S1). This matching suggests these simulations corresponded
 311 well with theory for continuous populations at equilibrium, despite ignoring the
 312 effects of negative density dependence, uneven distribution of individuals, and
 313 boundary effects (Nick H. Barton, Depaulis, and Etheridge 2002).

314 With increasing scale of gene flow we see a flatter change in wavelet dis-
 315 similarity across spatial scales (Figure S5 in File S1). When gene flow is local,
 316 wavelet dissimilarity is low at small scales and high at large scales. At the large
 317 gene flow scale, the observed wavelet dissimilarity is indistinguishable from the
 318 panmictic null. We also ran the same analyses but using biased sampling along
 319 the landscape's y-axis, so that 3/4 of samples were in the upper half of the land-
 320 scape. Even with this bias, the wavelet dissimilarities across scales and gene flow
 321 parameters were essentially unchanged (Figure S6 in File S1). To investigate
 322 sensitivity to landscape size, we also ran these same simulations with landscapes

323 four times as large (50x50) and found similar patterns of wavelet dissimilarity
 324 across scales and simulated gene flows (Figure S7 in File S1).

325 **3 Results**

326 **3.0.1 Simulated long-term neutral patterns in a heterogeneous land- 327 scape**

328 To assess if our approach could identify localized and scale-specific patterns of
 329 isolation by distance, we next simulated multiple scenarios where we expected
 330 spatial heterogeneity. First, we simulated neutral evolution across a simulated
 331 patchy landscape (generated from earlier work) (Jesse R. Lasky and Keitt 2013).
 332 This landscape contained a substantial portion of unsuitable habitat where ar-
 333 riving propagules perished. We used the same population parameters as previ-
 334 ously and simulated 100,000 time steps to reach approximately stable relatedness
 335 patterns. We then calculated wavelet dissimilarity using 1,000 random SNPs of
 336 200 sampled individuals.

337 Additionally, we sought to compare wavelet dissimilarities to more familiar
 338 metrics. To do so, we calculated euclidean genetic distance (in the space of
 339 allele frequencies across the genome) and geographic distance between pairs
 340 of samples, and did this for different subsets of samples and regions, so as
 341 to compare localized patterns in wavelet dissimilarity to localized patterns in
 342 pairwise distances.

343 In our landscape, wavelet dissimilarity showed localized and scale-specific
 344 patterns of low and high dissimilarity (Figure 2). Notably, the same two islands
 345 (top left and bottom right of landscape in Figure 2) have lower dissimilarity
 346 than expected at small scales and are more dissimilar than expected at larger
 347 scales. Stated another way, these islands have low diversity locally (e.g. within
 348 populations), as can be seen by the slow increase in genetic distance with geo-
 349 graphic distance locally (Figure 2D, compare to 2F). However, at larger scales
 350 (e.g. comparing island to mainland) islands are more dissimilar, as seen by the
 351 greater genetic distances at larger geographic distances (Figure 2E, compare to
 352 2G; also see the first two principal components of SNPs, Figure S8 in File S1).
 353 These results highlight the capacity of the method to contrast patterns across
 354 scales requiring only dilation of the analyzing kernel.

355 **3.0.2 Simulated neutral patterns in a colonizing and range- 356 expanding species**

357 For a second scenario where we expected localized, scale-specific heterogeneity,
 358 we simulated an invasion/range expansion. Beyond the importance of invasions
 359 in applied biology, the changes in spatial genetic patterns over time are of general
 360 interest (Castric and Bernatchez 2003; Le Corre et al. 1997; Slatkin 1991, 1993),
 361 considering that all species ranges are dynamic and many "native" species still
 362 bear clear evidence of expansion, e.g. following the last glacial maximum.

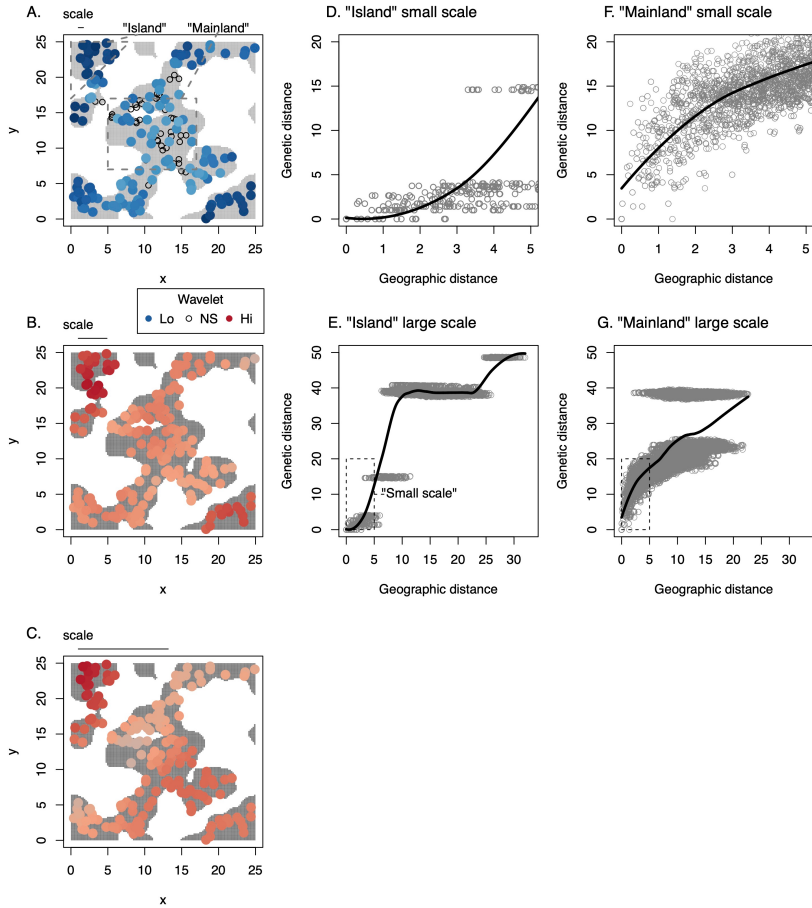


Figure 2: Wavelet genetic dissimilarity identifies scale-specific, localized patterns in a heterogeneous landscape, with pairwise distance plots for comparison. (A-C) Maps of simulated landscape where habitat is gray (in background) and unsuitable areas are white. Sampled individuals are circles. Colors represent sampling locations where wavelet genetic dissimilarity was significantly high (red) or low (blue), with s , the wavelet scale, shown at top of each panel as a horizontal line. At the smallest scales (A), samples have less dissimilarity than expected, especially in the island in the upper left of the landscape. This pattern can also be seen (D,F) when comparing pairwise geographic versus euclidean genetic distances for samples in the different regions of the landscape (dashed grey lines in A). At larger spatial scales (B-C), all locations have significantly greater dissimilarity than expected due to limited gene flow. However, the same islands show the greatest dissimilarity at large scales (lower panels), due to their high genetic difference from mainland samples at center. This pattern can also be seen in the pairwise genetic distances across larger geographic distances (E,G). (D-G) Loess smoothing curves are shown.

363 We simulated invasion across a square landscape of the same size as before,
 364 but beginning with identical individuals only in the middle at the bottom edge
 365 of the landscape (Figure 3). We sampled 200 individuals at time steps 100, 250,
 366 500, 1000, 1500, 2000, through the full populating of the landscape around 2500
 367 years and until the 3000th time step.

368 We characterized wavelet genetic dissimilarity and found substantial hetero-
 369 geneity across different regions and across time (e.g. for $s = 6.9$, dark versus
 370 light red in Figure 3A-C). This heterogeneity in genetic turnover can be seen by
 371 contrasting genotypes from different regions. Near the expansion front, there
 372 is relative homogeneity and low diversity locally in new populations, but with
 373 rapid turnover in genotypes separated by space, resulting in high wavelet dis-
 374 similarity at intermediate spatial scales (Figure 3D). In the range interior, there
 375 is greater local diversity and less turnover in genotype across space, i.e. a weaker
 376 isolation by distance (Figure 3E, see all SNP genetic distance plot Figure S9 in
 377 File S1). Supporting the role of founder effects and low diversity at expanding
 378 range margins in driving these patterns, we observed a decline in medium- and
 379 large-scale wavelet dissimilarity in later years (Figure 3G) after the landscape
 380 had been populated.

381 These patterns highlight how wavelet dissimilarity is capturing scale-specific
 382 turnover in genetic composition, rather than merely genetic distance at a given
 383 geographic distance. Comparing the two regions highlighted in Figure 3B, the
 384 genetic distances at a geographic distance of 6.9 are not strikingly different
 385 (Figure S9 in File S1). Rather what distinguishes these regions is their rate
 386 of genetic change in composition at this scale, as highlighted in Figure 3. The
 387 region of high wavelet dissimilarity at $s = 6.9$ (Figure 3B) transitions from
 388 homogeneity among nearby samples to high genetic distance at larger scales
 389 (Figure 3D, S9). By contrast the region of low wavelet dissimilarity at $s = 6.9$
 390 (Figure 3B) starts out with greater genetic distance among nearby samples with
 391 a modest increase in genetic distance at larger scales (Figure 3E, S9).

392 Overall, these simulations show the capacity of $D_{a,b}^{wav}(s)$, wavelet genetic
 393 dissimilarity, to capture localized, scale specific trends in genetic composition.
 394 Given the spatial heterogeneity in nature and the dynamics of populations and
 395 species ranges through time, there are likely many such patterns waiting to be
 396 described to shed light on patterns of gene flow and population history.

397 3.1 Finding the loci of local adaptation

398 3.1.1 Using wavelet transforms to identify outliers of spatial pattern 399 in allele frequency

400 We can also use our approach to transforming allele frequencies to identify par-
 401 ticular genetic loci involved in local adaptation, and the regions and spatial
 402 scales of turnover in their allele frequency. Our strategy is (as before) to first
 403 calculate $(T^{wav} f_i)(a, b, s)$, the wavelet transform, for each locus i at each sam-
 404 pling point a, b for a set of chosen spatial scales $s \in S$.

405 Because of different ages and histories of drift, mutations will vary in their

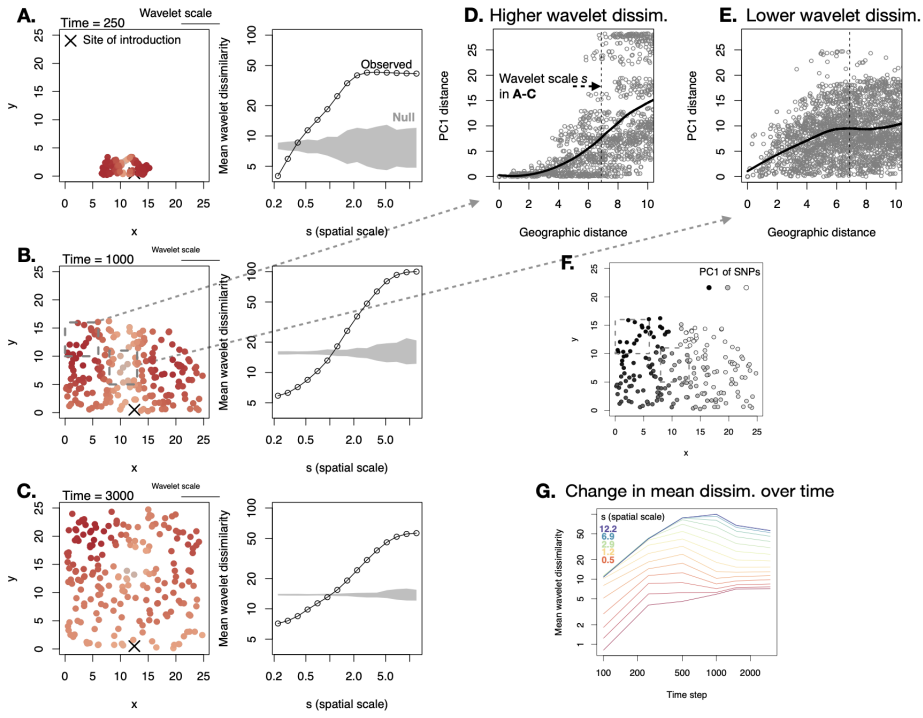


Figure 3: Wavelet genetic dissimilarity reveals dynamic spatial patterns during an invasion across a homogeneous landscape. Left column of panels (A-C) shows a map of the landscape through time, with 200 sampled individuals at each time step and the wavelet dissimilarity at $s = 6.9$ at their location. Darker red indicates greater wavelet dissimilarity. In the second time step, 1000, two regions are highlighted in dashed boxes (B), one with higher dissimilarity at $s = 6.9$ (D) and one with lower dissimilarity at this scale (E). (D-E) show pairwise geographic distance versus distance in the first PC of SNPs for samples from these regions. (F) shows the loadings of each sample on the first PC of SNPs. (D-E) highlight the greater increase in PC1 distance with geographic distance at this scale (vertical dashed lines) in (D), compared to the smaller increase in PC1 distance at this scale in (E). In particular, the region highlighted in (D) is homogeneous at short distances but very distinct at distances at the highlighted scale $s = 6.9$, indicating the major genetic turnover at this scale and location. (G) Mean wavelet dissimilarity across the landscape changes over time, highlighting the dynamic spatial population genetic patterns across invasions. Loess smoothing curves are shown in (E-F).

406 global allele frequency and thus global variance. To facilitate comparisons
 407 among loci for relative evidence of selection, we can normalize spatial patterns in
 408 allele frequency by total variation across locations, as is done when calculating
 409 F_{ST} .

410 Here we divide the wavelet transforms of allele frequency by the standard
 411 deviation of global allele frequency variation for each locus i , $sd(f_i)$. This nor-
 412 malization is greatest when minor allele frequency is 0.5 for a biallelic locus, and
 413 yields a scaled wavelet transformed allele frequency: $(T^{wav}f_i)(a, b, s)/sd(f_i)$, for
 414 a given location and scale.

415 We then calculate the variance across sampling locations of
 416 $(T^{wav}f_i)(a, b, s)/sd(f_i)$ and refer to this quantity as the "scale-specific
 417 genetic variance." This scaled-specific variance is akin to F_{ST} in being a
 418 measure of spatial variation in allele frequency normalized to total variation
 419 (which is determined by mean allele frequency). High scale-specific variance
 420 for a given locus indicates high variation at that scale relative to the total
 421 variation and mean allele frequency. We then used a χ^2 null distribution across
 422 all genomic loci to calculate parametric p-values (Cavalli-Sforza 1966; Lewontin
 423 and Krakauer 1973) and used the approach of Whitlock and Lotterhos (2015) to
 424 fit the degrees of freedom of the distribution of scale-specific genetic variances
 425 (see Supplemental Methods). Applying this approach to a range of simulated
 426 scenarios as well as an empirical dataset (described below), we see that the χ^2
 427 distribution with a maximum likelihood fit to determine degrees of freedom
 428 provides a reasonably close fit to the distribution of scale-specific genetic
 429 variance among SNPs (Figures S10-S13 in File S1).

430 3.1.2 Simulated local adaptation

431 First, we present some specific individual simulations for illustration, and then
 432 a larger set with more variation in underlying parameters. We simulated a
 433 species with the same life history parameters as in simulations above, with
 434 the addition of spatially varying viability selection on a quantitative trait. We
 435 imposed two geometries of spatially varying selection, one a linear gradient
 436 and the other a square patch of different habitat selecting for a different trait
 437 value. As with the neutral simulations, simulations with selection began with
 438 organisms distributed across the landscape, with an ancestral trait value of
 439 zero. In these simulations, 1% of mutations influenced the quantitative trait
 440 with additive effects and with effect size normally distributed with a standard
 441 deviation of 5. For the linear gradient, the optimal trait value was 0.5 at one
 442 extreme and -0.5 at the other extreme, on a 25x25 square landscape. Selection
 443 was imposed using a Gaussian fitness function to proportionally reduce survival
 444 probability, with standard deviation σ_k . In this first simulation, $\sigma_k = 0.5$.
 445 Carrying capacity was roughly 5 individuals per square unit area, and simulated
 446 populations usually stabilized close to this density. Full details of simulation,
 447 including complete code, can be found in supplemental materials and on GitHub
 448 (<https://github.com/jesserlasky/WaveletSpatialGenetic>).

449 In the first simulation along a linear gradient after 2,000 time steps there

450 were 2 selected loci with minor allele frequency (MAF) at least 0.1, with a
 451 genetic variance in the trait of 3.7. (the scale of mating and propagule dispersal
 452 were each $\sigma = 1.1$) The two loci under stronger selection were clearly identified
 453 by the scale-specific genetic variance $\text{var}((T^{\text{wave}} f_i)(a, b, s)/sd(f_i))$ at the larger
 454 spatial scales (Figure 4). When there is a linear selective gradient across the
 455 entire landscape, the largest spatial scale is the one most strongly differentiating
 456 environments and the strongest scale-specific genetic variance was at the largest
 457 scale (Figure 4). However, power may not be greatest at these largest scales,
 458 because population structure also is greatest at these largest scales. Instead,
 459 power was greatest at intermediate scales, as seen by the lowest p-values being
 460 detected at these intermediate scales (Figure 4). At these scales there is greater
 461 gene flow but still some degree of changing selection that may maximize power
 462 to detect selection.

463 We next simulated change in selection in a discrete habitat patch, which
 464 may more closely correspond to the setting where researchers would find useful
 465 a flexible approach to finding spatial patterns in allele frequency, especially
 466 if the patches of distinct environment are not known by researchers. In our
 467 simulation there was a large central patch, 10x10, that selected for distinct trait
 468 values (trait optimum = 0.5) compared to the outer parts of the landscape (trait
 469 optimum = -0.5). Selection was initially weakly stabilizing ($\sigma_k = 3$ around the
 470 optimum of zero for the first 500 years to accumulate diversity, and then the
 471 patch selective differences were imposed with stronger selection, $\sigma_k = 0.08$. The
 472 scales of mating and propagule dispersal were each $\sigma = 2$. Carrying capacity
 473 was roughly 50 individuals per square unit area.

474 In this simulation we present results after 3000 time steps, where there was
 475 a single common QTL under selection, giving a genetic variance in trait of 0.42
 476 (Figure 5). We found several spurious large scale peaks in scale-specific genetic
 477 variance (Figure 5A), but when using the χ^2 test on these statistics we clearly
 478 identified the single QTL under selection, with lowest p-values for intermediate
 479 scales (Figure 5B).

480 We calculated the scale-specific genetic variance across a denser spectrum
 481 of scales s for the causal SNP, to determine at what scale variance was greatest.
 482 We found the maximum scale-specific genetic variance for the causal SNP
 483 was at 5.02, approximately half the length of a patch edge (Figure 5C). For
 484 illustration, we also calculated F_{ST} (Goudet 2005; Weir and Cockerham 1984)
 485 for several naively discretized subpopulation scenarios for a simple illustration
 486 of how results are sensitive to discretization (Figure 5D-F). We also implement
 487 our test on these two simulated landscapes but with biased sampling and found
 488 our ability to detect causal loci was robust (Figure S14 in File S1).

489 3.1.3 Evaluating the scale-specific genetic variance test

490 As an initial assessment of the general appropriateness of the scale-specific ge-
 491 netic variance test we proposed above, we conducted additional simulations on
 492 two types of landscapes with varying life history parameters. These simulations
 493 were not meant to be an exhaustive evaluation of the performance of this new

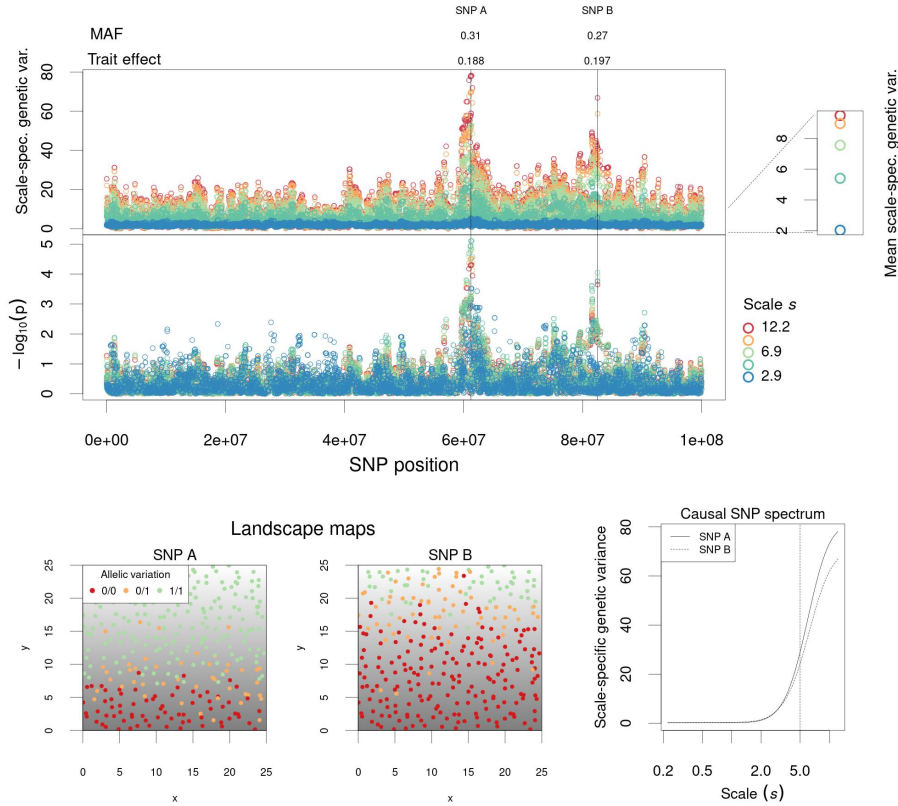


Figure 4: Scale-specific genetic variance test applied to simulations with a linear selective gradient. (top panels) Genome-wide variation in scale-specific genetic variance, $\text{var}((T^{w a v} f_i)(a, b, s)/\text{sd}(f_i))$, for five different scales s and upper-tail p-values for χ^2 test using fitted values of d.f. Each point represents a SNP at a specific scale. Loci under selection are indicated with vertical lines along with the absolute value of the derived allele's effect on the trait and MAF. At bottom are shown maps of the two selected loci as well as their spectra of scale-specific genetic variance. At upper right the mean scale-specific genetic variance across all genomic loci is shown for each scale s . The scale of mating and propagule dispersal were each $\sigma = 1.1$. Gaussian viability selection was imposed with $\sigma_k = 0.5$. Carrying capacity was approximately 5 individuals per square unit area.

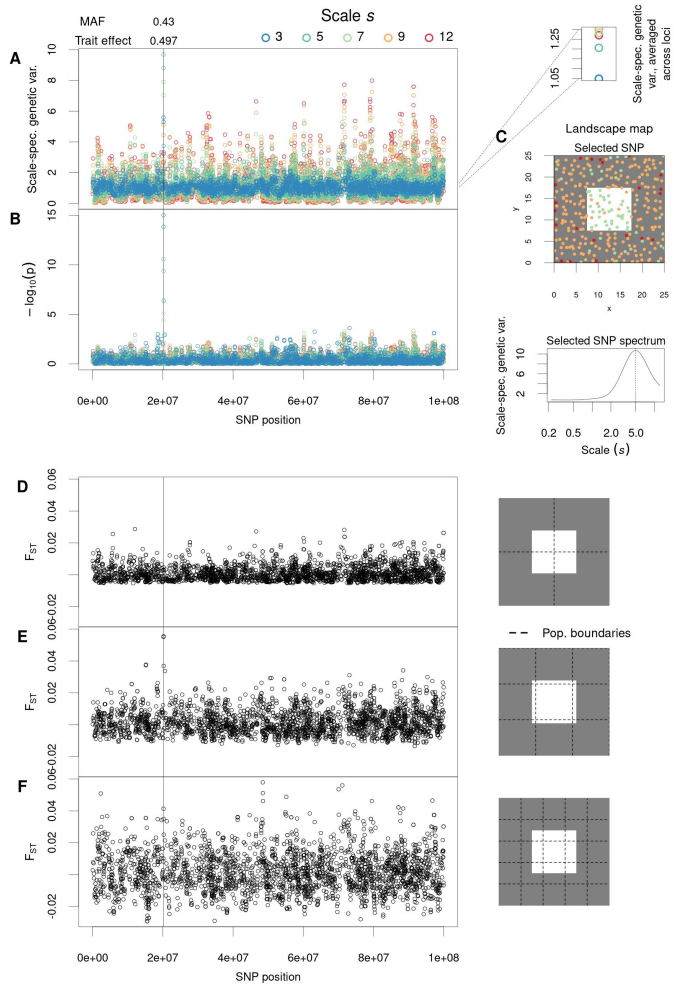


Figure 5: Simulations of local adaptation to a single discrete patch of different habitat. (A) Genome-wide variation in scale-specific genetic variance $\text{var}((T^{\text{wave}} f_i)(a, b, s)/\text{sd}(f_i))$ and (B) χ^2 p-values for six different scales s , for a discrete habitat difference after 3000 simulated years. Each point in the left panels represents a SNP, and wavelet statistics (A-B) at specific scales. The selected SNP is indicated with a vertical line along with the absolute value of a derived allele's effect on the trait and MAF. (C) A map of the landscape with individuals' genotypes at the causal SNP indicated with color, in addition to the spectrum of scale-specific genetic variance at this SNP, showing a peak at approximately half the patch width (vertical line at 5). (D-E) Implementation of F_{ST} using arbitrary boundaries for populations. This approach can easily miss causal loci (C,E) if the delineated population boundaries do not match habitat boundaries. (A) At upper right the mean scale-specific genetic variance across all loci is shown for each scale s . The scale of mating and propagule dispersal were each $\sigma = 2$. Gaussian viability selection was imposed with $\sigma_k = 0.08$.

494 test; we leave a more extensive evaluation for future studies.

495 Here, we again used the discrete habitat patch landscape and the linear
 496 gradient landscape but with a wider range of parameter variation. We tested
 497 a range of mating and dispersal (σ) scales including 0.25, 0.5, 1, and 2, and a
 498 range of stabilizing selection (σ_k) values including 0.125, 0.25, 0.5, and 1. Three
 499 simulations were conducted for each combination of parameter settings and each
 500 ran for 10,000 years.

501 Because PCAdapt is one of the few methods for identification of spatial
 502 pattern in allele frequency that does not require subpopulation discretization
 503 and in theory could detect patterns at multiple scales, we also implemented
 504 this method. We used the PCA of the scaled genotype matrix, thinned for
 505 LD but including causal SNPs, to extract the z-scores and p-values of each
 506 SNP with a cutoff of $p = 0.05$. We used a scree plot showing the percentage
 507 of variance explained in decreasing order to identify the optimal number of
 508 principal components following Cattell's rule (Duforet-Frebourg et al. 2016).

509 Calculating false and true positive rates for PCAdapt was straightforward,
 510 but for the scale specific genetic variance test there are several tests (one at
 511 each scale) for each SNP. To conservatively represent inference across these
 512 multiple tests, we considered SNPs a significant result if one of the tested scales
 513 was significant. Because the individual scale tests are slightly conservative,
 514 and continuous wavelet transforms are correlated across scales (and hence not
 515 completely independent tests), we expected the resulting false positive rates
 516 would not be unduly high.

517 Overall the scale-specific genetic variance test showed good false positive
 518 rates. Across simulations, the proportion of SNPs with χ^2 upper-tail $p < 0.05$
 519 at one scale was usually close to but sometimes slightly more than 0.05 (Figure
 520 6). By contrast, under scenarios of low gene flow and strong stabilizing selection,
 521 nominal false positive rates were high for PCAdapt, often > 0.15 .

522 Power to detect SNPs (proportion of selected SNPs with $p < 0.05$) under
 523 selection was generally high (true positive rate near 1) but sometimes low, de-
 524 pending on the strength of selection (σ_k) and mating and dispersal scales (σ)
 525 (Figure 6). When gene flow was high and selection was weak, power was low
 526 for both the scale-specific genetic variance test and PCAdapt. This also corre-
 527 sponds to the scenario when local adaptation is weakest (Kirkpatrick and N. H.
 528 Barton 1997). In addition to considering power simply based on p for each SNP,
 529 we also considered power using the top p -value rank among selected SNPs under
 530 each simulation, based on the reasoning that researchers may want to follow up
 531 on top ranked outlier SNPs first before any lower ranked SNPs. This approach
 532 showed similar results, with high power for both the scale-specific genetic vari-
 533 ance test and PCAdapt except when gene flow was high and selection weak. In
 534 general, the two methods showed comparable power across different scenarios
 535 (Figure 6), with some indication that the scale-specific genetic variance test had
 536 higher power under high gene flow and PCAdapt slightly higher power under
 537 lower gene flow. By plotting individual SNPs we can see that for the upper end
 538 of gene flow scenarios ($\sigma = 1$ or 2), the scale-specific genetic variance test more
 539 consistently identified selected SNPs at the top compared to PCAdapt. For the

540 low gene flow scenarios, PCAdapt more consistently identified large effect variants,
 541 while the scale-specific genetic variance test more consistently identified
 542 the smaller effect variants (see results for linear gradient in Figure S15 in File
 543 S1). Overall, the similarities in true and false positive rates between methods
 544 suggest that our wavelet approach is effective compared to other related tools,
 545 while our test also offers the ability to explicitly consider variation in spatial
 546 scale.

547 3.2 Testing for spatial pattern in quantitative trait loci 548 (QTL)

549 When testing for spatially-varying selection on a quantitative trait, one approach
 550 is ask whether QTL identified from association or linkage mapping studies show
 551 greater allele frequency differences among populations than expected (Berg and
 552 G. Coop 2014; Price et al. 2018). Here we implement such an approach to
 553 compare wavelet transformed allele frequencies for QTL L to a set of randomly
 554 selected loci of the same number and distribution.

555 For this test we calculate the mean of scale-specific genetic variance for all
 556 QTL with MAF at least 0.05 among sampled individuals. We then permute
 557 the identity of causal QTL across the genome and recalculate the mean scale-
 558 specific genetic variance, and repeat this process 1000 times to generate a null
 559 distribution of mean scale-specific genetic variance of QTL for each scale s .

560 We illustrate this test here briefly using a simulation of adaptation to a
 561 square patch of habitat in the middle of a landscape, with the two gene flow
 562 parameters $\sigma = 0.5$, the strength of selection $\sigma_K = 0.5$, carrying capacity
 563 ~ 5 individuals per square unit area. After 1000 generations we sampled 300
 564 individuals, from which there were 13 QTL for the trait under selection with
 565 MAF at least 0.05. We then calculated the mean scale-specific genetic variance
 566 for these QTL across scales s and compared to the null permutations of randomly
 567 selected 13 SNPs from the genome.

568 We found significantly higher mean scale-specific genetic variance for the
 569 QTL than the null expectation at all 6 scales tested. Although the scale-specific
 570 genetic variance was greatest at the largest scales for the QTL, these scales did
 571 not show as great a distinction when comparing to the null. The greatest mean
 572 wavelet variance of QTL relative to null came at the intermediate scales of 3-5,
 573 which was approximately 1/3-1/2 the width of the habitat patch (Figure S16 in
 574 File S1).

575 3.3 Application to an empirical system

576 3.3.1 Genome-wide wavelet dissimilarity

577 We applied our approach to an empirical dataset of diverse, broadly distributed
 578 genotypes with whole genome resequencing data: 908 genotypes from 680 nat-
 579 ural populations of the model plant, *Arabidopsis thaliana* (Brassicaceae). We

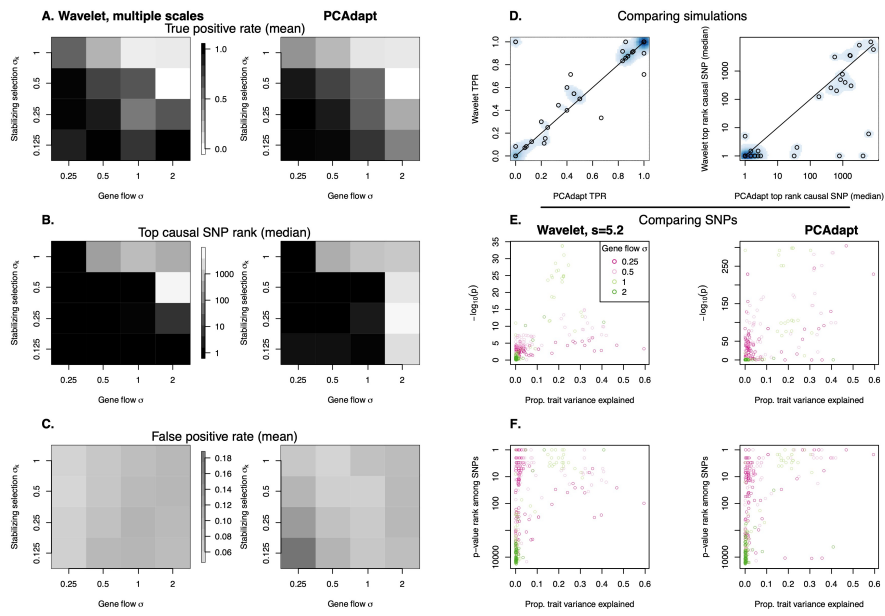


Figure 6: Comparing the scale-specific genetic variance test with PCAdapt in simulations of adaptation to single discrete patch of different habitat. (A) True positive rates (nominal $p < 0.05$) for each combination of simulation parameters, the scales of mating and dispersal σ and the standard deviation of the Gaussian stabilizing selection function σ_k . (B) An alternate view of statistical power based on the median rank of the top selected SNP among all SNPs. (C) False positive rates (nominal $p < 0.05$). (D) Comparing power between the two statistical approaches for the different simulation runs. Density of points is shown in the blue scale so as to indicate where many simulations had the same result. The line indicates a 1:1 relationship. (E-F) Individual selected SNPs in simulations, showing their nominal p values and ranks among all SNPs, colored based on σ in the simulation. The x-axis represents the proportion of total phenotypic variation among sampled individuals that was explained by the given SNP (R^2 from a linear model).

580 used a published Arabidopsis dataset (Alonso-Blanco et al. 2016), only including
 581 Eurasian populations and excluding highly distinct "relicts" and also likely
 582 contaminant accessions (Pisupati et al. 2017). For locations with more than one
 583 accession genotyped we calculated allele frequency. We used a total of 129536
 584 SNPs filtered for minor allele frequency ($MAF > 0.05$) and LD (Zheng et al.
 585 2012).

586 We first calculated the genome-wide wavelet dissimilarity, $D_{a,b}^{wav}(s)$, across a
 587 series of increasing scales s at even intervals in log distance units from ~ 50 m
 588 to approximately half the distance separating the farthest samples, ~ 3000 km.

589 We observed increasing mean genome-wide wavelet dissimilarity at larger
 590 scales (Figure 7), a pattern indicative of isolation by distance, on average, across
 591 the landscape. Arabidopsis showed significantly low dissimilarity at scales less
 592 than ~ 5 km, likely due to the homogenizing effect of gene flow. However, we
 593 found significantly high dissimilarity at scales greater than ~ 7 km. This scale
 594 of significantly high dissimilarity may be a relatively short distance, consider-
 595 ing that Arabidopsis is largely self pollinating and lacks clear seed dispersal
 596 mechanisms (though seeds of some genotypes form mucus in water that increases
 597 buoyancy) (Saez-Aguayo et al. 2014). At scales greater than ~ 120 km we found
 598 an increase in the slope relating scale s and dissimilarity, perhaps signifying a
 599 scale at which local adaptation begins to emerge.

600 The locations of scale-specific dissimilarity among Arabidopsis populations
 601 revealed several interesting patterns. Even by the ~ 30 km scale, there were
 602 three notable regions of significantly high dissimilarity: northern Spain and
 603 extreme southern and northern Sweden (Figure 7). The high dissimilarity at this
 604 scale in northern Spain corresponds to the most mountainous regions of Iberia,
 605 suggesting that limitations to gene flow across this rugged landscape have led
 606 to especially strong isolation among populations at short distances. In northern
 607 Sweden, Long et al. (2013) previously found a particularly steep increase in
 608 isolation-by-distance. Alonso-Blanco et al. (2016) found that genetic distance
 609 was greatest among accessions from Southern Sweden at scales from $\sim 20 - 250$
 610 compared to regions farther south. At larger, among-region scales, dissimilarity
 611 was significantly high across the range, with Iberia and northern Sweden again
 612 being most dissimilar at ~ 234 km and surpassed by central Asia at ~ 1834 km
 613 as being most dissimilar. Iberia and northern Sweden contain many accessions
 614 distantly related to other accessions, likely due to isolation during glaciation
 615 and subsequent demographic histories (Alonso-Blanco et al. 2016). This scale
 616 in Asia separates populations in Siberia from those further south in the Tian
 617 Shan and Himalayas, indicating substantial divergence potentially due to limited
 618 gene flow across the heterogeneous landscape. By contrast, populations in the
 619 UK and the Balkan peninsula had low dissimilarity across a range of scales,
 620 possibly due to reduced diversity and a more recent history of spread in these
 621 regions.

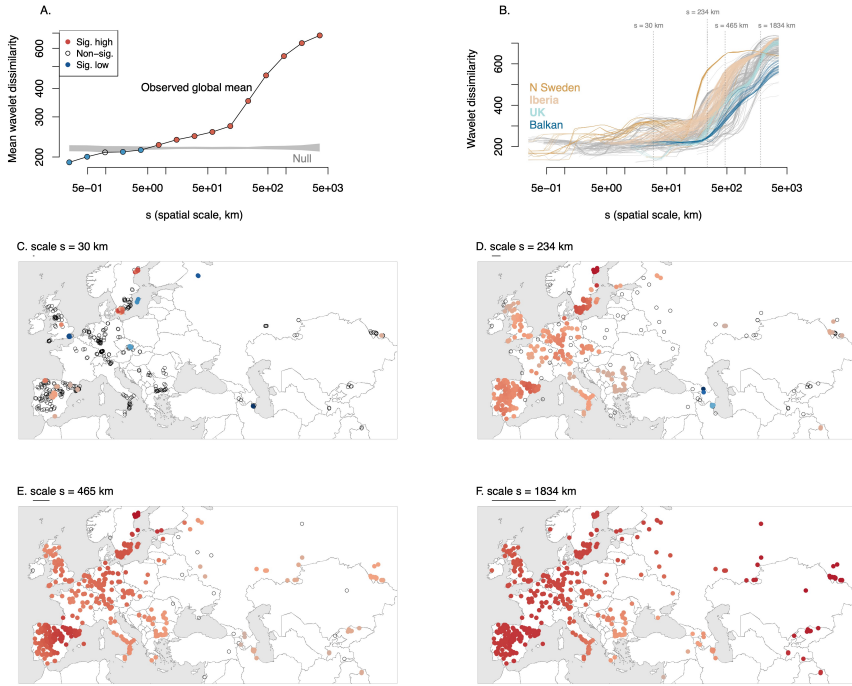


Figure 7: Genome-wide wavelet dissimilarity, $D_{a,b}^{wav}(s)$, for *Arabidopsis* genotypes. (A) The global mean dissimilarity across scales compared to the null expectation (gray ribbon) and (B) the dissimilarity across scales centered on each sampled genotype, with several regions highlighted (vertical lines indicate scales shown in panels C-F). (C-F) Selected scales highlight the changes in dissimilarity across locations, with each circle indicating a genotyped sample/population. Red indicates significantly greater wavelet dissimilarity than expected, blue significantly less than expected. For the map panels, the intensity of color shading indicates the relative variation (for a given scale) in $D_{a,b}^{wav}(s)$ among significant locations.

622 **3.3.2 Identifying putative locally-adapted loci**

623 For this analysis, we used the same genotypes as in the prior section but not
 624 filtered for LD, leaving 1,642,040 SNPs with MAF> 0.1 (Alonso-Blanco et al.
 625 2016).

626 The scale-specific genetic variance test identified putative locally adapted
 627 loci (Figure S17 in File S1). The distribution of scale-specific genetic variance
 628 among SNPs was reasonably matched to the theoretical χ^2 distribution (Figure
 629 S13 in File S1). Among notable loci, at the ~ 59 km scale, the #2 QTL and #3
 630 SNP is in the coding region of METACASPASE 4 (MC4), a gene that controls
 631 biotic and abiotic stress-induced programmed cell death (Hander et al. 2019;
 632 Shen, Liu, and Li 2019). To speculate, if MC4 were involved in coevolution
 633 with microbial pathogens we might expect rapid allele frequency dynamics and
 634 thus a pattern of high variation among even nearby populations.

635 The #1 SNP for the ~ 282 km scale was in the coding sequence of the DOG1
 636 gene (Figure 8, Figure S17 in File S1). This SNP, Chr. 5, 18,590,741 was also
 637 strongly associated with flowering time (see next section) and germination and
 638 tags known functional polymorphisms at this gene that are likely locally adaptive
 639 (Martínez-Berdeja et al. 2020). The spatial pattern of variation at this
 640 locus (Figure 8) is complicated, highlighting the benefit of the flexible wavelet
 641 approach. By contrast, imposing a grid on this landscape, or using national
 642 political boundaries to calculate F_{ST} could easily miss the signal as did Horton
 643 et al. (2012). The climate-allele frequency associations for DOG1 are also com-
 644 plicated and non-monotonic (**gamba`genomics`2023** ; Martínez-Berdeja et al.
 645 2020), making it challenging for genotype-environment association approaches
 646 (Jesse R Lasky, Emily B Josephs, and Morris 2023).

647 At the ~ 1359 km scale, the #1 SNP (and also the lowest p-value SNP among
 648 all scales, Figure 8, Figure S17 in File S1) was on chromosome 5 at 26,247,515 bp,
 649 555 bp upstream from AT5G65660, a hydroxyproline-rich glycoprotein family
 650 protein. These are cell wall glycoproteins with important roles in development
 651 and growth (Johnson et al. 2017) some of which have a role in abiotic stress
 652 response (Tseng et al. 2013).

653 **3.3.3 Testing for local adaptation in quantitative trait loci (QTL)**

654 We tested for non-random scale-specific genetic variance of QTL for Arabidopsis
 655 flowering time, a trait that is likely involved in local adaptation (Ågren et al.
 656 2017). We used previously published data on flowering time: days to flower at
 657 10°C measured on 1003 genotypes and days to flower at 16°C measured on 970
 658 resequenced genotypes (Alonso-Blanco et al. 2016). We then performed mixed-
 659 model genome wide association studies (GWAS) in GEMMA (v 0.98.3) (Zhou
 660 and Stephens 2012) with 2,048,993 M SNPs filtered for minor allele frequency
 661 (MAF> 0.05), while controlling for genome-wide similarity among ecotypes.

662 We found that top flowering time GWAS SNPs showed significantly elevated
 663 scale-specific genetic variance at several intermediate spatial scales tested. For
 664 flowering time at both 10° and 16°C, scale-specific genetic variance was signifi-

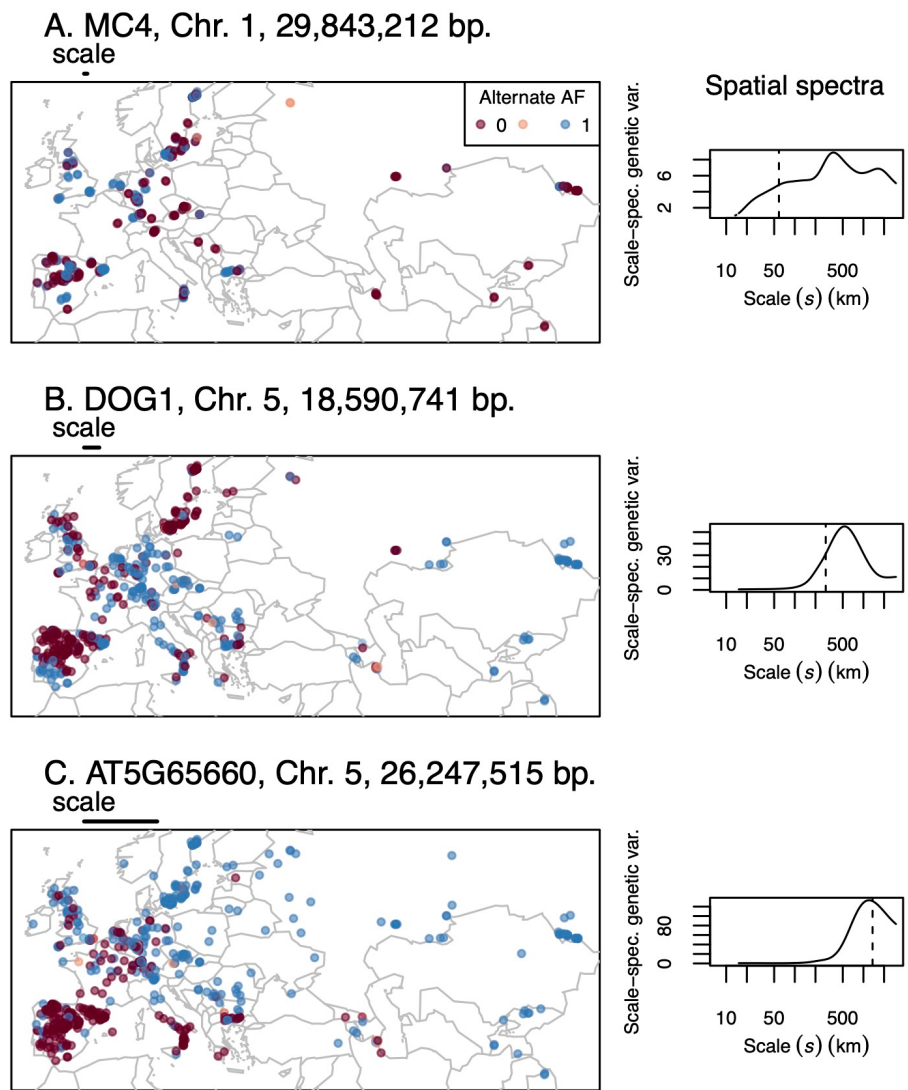


Figure 8: Allelic variation (colors) for SNPs that were top outliers for scale-specific genetic variance test at different scales. On maps at left, the scale for which a SNP was an outlier is indicated by a bar above each map. The right panels show the spatial spectra for each SNP, i.e. the scale-specific genetic variance across a range of scales. Dashed lines indicate the scale for which a SNP was an outlier.

665 cantly elevated for the top 1,000 SNPs at the 282, 619, and 1359 km scales, but
 666 not always at the largest or smallest scales (Figure 9). In particular the scale-
 667 specific genetic variances were greatest for the ~ 282 km scale where the mean
 668 scale specific genetic variance for 16°C QTL was 15.2 standard deviations above
 669 the null mean, and the ~ 619 km scale, where the mean scale specific genetic
 670 variance for 10°C QTL was 13.5 standard deviations above the null mean. For
 671 QTL from both temperature experiments, results were nearly equivalent if we
 672 instead used the top 100 SNPs.

673 4 Discussion

674 Geneticists have long developed theory for spatial patterns in allele frequency
 675 (Haldane 1948; Malécot 1948; Wright 1943). Empiricist have sought to use these
 676 patterns make inference about underlying processes of demography, gene flow,
 677 and selection (Lewontin and Krakauer 1973; McRae et al. 2008; Rousset 2000).
 678 While statistical approaches have been developed to characterize geographic
 679 patterns, few are flexible enough to incorporate patterns at a range of scales that
 680 are also localized in space. Because wavelet transforms have these properties,
 681 we think they may be useful tools for geneticists. Here we demonstrated several
 682 applications of wavelet transforms to capture patterns in whole genome variation
 683 and at particular loci, under a range of neutral and non-neutral scenarios.

684 Some important existing approaches are based on discretization of spatially-
 685 distributed samples into spatial bins, i.e. putative populations (Bishop, Cham-
 686 bers, and I. J. Wang 2023; Petkova, Novembre, and Stephens 2016; Weir and
 687 Cockerham 1984). However, without prior knowledge of selective gradients, pat-
 688 terns of gene flow, or relevant barriers, it is often unclear how to delineate these
 689 populations. For example, we can see how the specific discretization can hinder
 690 our ability to find locally-adapted loci in our simulations (Figure 5) and in em-
 691 pirical studies of *Arabidopsis* in the case of the phenology gene DOG1 that was
 692 missed in previous F_{ST} scans (Alonso-Blanco et al. 2016; Horton et al. 2012).

693 Our goal in this paper was to provide a new perspective on spatial popula-
 694 tion genetics using the population-agnostic, and spatially smooth approach of
 695 wavelet transforms. We showed how these transforms characterize scale-specific
 696 and localized population structure across landscapes (Figures 2, 3, 7). We also
 697 showed how wavelet transforms can capture scale-specific evidence of selection
 698 on individual genetic loci (Figures 4, 5, 6, 8) and on groups of quantitative trait
 699 loci (Figure 9). Our simulations and empirical examples showed substantial
 700 heterogeneity in the scale and stationarity of spatial patterns. For example,
 701 the wavelet genetic dissimilarity allowed us to identify regions near a front of
 702 range expansion with steeper isolation by distance at particular scales due to
 703 drift (Figure 3). Additionally, we identified loci underlying local adaptation
 704 and showed an example where the evidence for this adaptation was specific to
 705 intermediate spatial scales (Figure 5). While existing approaches to character-
 706 izing population structure or local adaptation have some ability to characterize
 707 scale specific patterns, e.g. those based on ordinations of geography (Wagner,

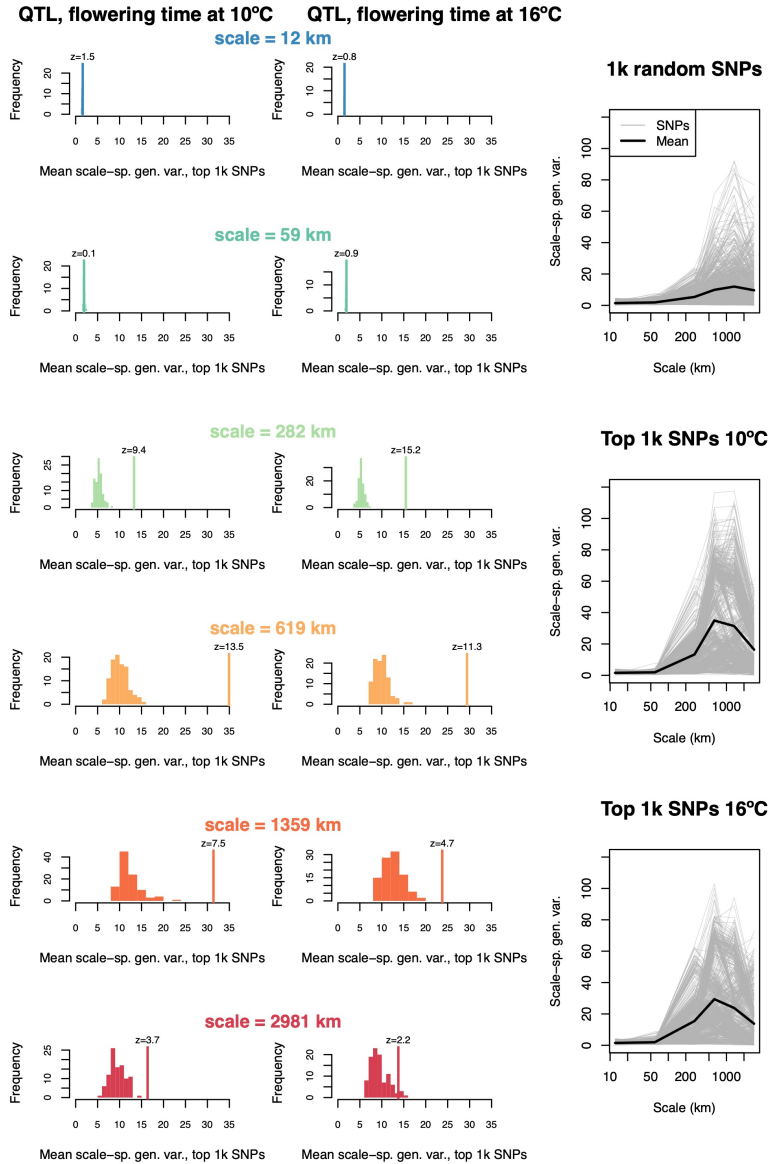


Figure 9: Testing for selection on *Arabidopsis* flowering time QTL. We compared scale-specific genetic variance, $\text{var}((T^{\text{wave}} f_i)(a, b, s)/\text{sd}(f_i))$, of QTL with random SNPs, for five different scales s , for flowering time measured at 10°C and 16°C. The first two columns show the observed mean of the top 1,000 flowering time SNPs with a vertical line and a z-score. The histograms show null distributions of scale-specific genetic variance based on permutations of an equal number of markers with an equal distribution as the flowering time QTL. At right the scale-specific genetic variance is shown for random SNPs and for the flowering time QTL (gray lines), across scales, with the mean indicated by a black line.

708 Chávez-Pesqueira, and Forester 2017) or SNPs (Emily B. Josephs et al. 2019),
 709 and some can capture localized patterns (e.g Petkova, Novembre, and Stephens
 710 2016), there are few examples of approaches that merge both abilities (Wagner,
 711 Chávez-Pesqueira, and Forester 2017).

712 Like many methods in population genetics that rely on inference from ob-
 713 servational data, we view our approaches as exploratory and hypothesis gen-
 714 erating. Heterogeneous patterns of genome-wide wavelet dissimilarity suggest
 715 demographic hypotheses, some of which can be tested with detailed ecological
 716 and genetic study (e.g. Keeley et al. 2017). For genome-scans for loci involved
 717 in local adaptation, the p-values resulting from multiple tested scales are compa-
 718 rable and so we recommend starting with the loci having the lowest p-value, and
 719 using these to develop hypotheses for functional follow up experiments (Jesse R
 720 Lasky, Emily B Josephs, and Morris 2023).

721 The test for spatial pattern in individual loci we developed owes greatly to
 722 previous work from Lewontin and Krakauer (1973) who initially developed χ^2
 723 tests applied to the distribution of F_{ST} values, and from Whitlock and Lotterhos
 724 (2015)'s approach of inferring the degrees of freedom of the χ^2 distribution
 725 using maximum likelihood and F_{ST} across loci. The χ^2 distribution underlies
 726 a number of related genetic applied across loci (François et al. 2016). However,
 727 we note that this test may be slightly conservative in some situations (Figure 6).
 728 Nevertheless, we believe there were important signs in our work that this χ^2 -
 729 based scale-specific genetic variance test was valuable. In particular, we found
 730 in our simulation of adaptation to a habitat patch that the scale-specific genetic
 731 variance was greatest at large spatial scales but at neutral sites, which obscured
 732 spatial pattern at the causal locus (Figure 5). When applying the χ^2 test, we
 733 were able to clearly map the causal locus while spurious loci with high scale-
 734 specific genetic variance fell away because spatial patterns at those loci still fit
 735 within the null distribution.

736 Relatedly, we found in other simulations and our empirical examples that the
 737 strongest evidence for local adaptation was often not at the largest spatial scales
 738 (Figure 9), even when the selective gradient was linear across the landscape (i.e.
 739 the largest scale, Figure 4). This enhanced power at scales sometimes smaller
 740 than the true selective gradients may be due to the limited power to resolve
 741 true adaptive clines at large scales from the genome-wide signal of isolation by
 742 distance at these scales. At intermediate scales, there may be a better balance
 743 of sufficient environmental variation to generate spatial pattern versus higher
 744 relatedness between locations due to gene flow.

745 We note that there remain several limitations to our approach proposed
 746 here. First, the ability of wavelet transforms to capture patterns depends on
 747 the correspondence between the wavelet form (shape) and the form of the em-
 748 pirical patterns we seek to enhance, and there may be better functional forms to
 749 filter spatial patterns in allele frequency. Generally speaking, a more compact
 750 smoothing kernel with minimum weight in the tails will be better at reveal-
 751 ing abrupt spatial transitions, but at the necessary cost of less precise deter-
 752 mination of scale (Heisenberg 1927). Smoothing kernels such as the tricube

($k_x \simeq [1 - x^3]^3$) have been shown to optimize certain trade-offs in this space and could be used to construct a difference-of-kernels wavelet. However, the overall influence of kernel shape tends to be much less than the influence of kernel bandwidth in our experience. Second, we have not yet implemented localized tests for selection (i.e. specific to certain locations) as we did with genome-wide dissimilarity. A challenge applying this test at individual loci is that there is a very large number of resulting tests from combinations of loci, locations, and scales. Therefore we have not fully exploited the localized information we derive from the wavelet transforms.

There are number of interesting future directions for research on wavelet characterization of spatial pattern in evolutionary biology. First, we could apply the wavelet transforms to genetic variation in quantitative traits measured in common gardens, to develop tests for selection on traits akin to the Q_{ST} - F_{ST} test (Emily B. Josephs et al. 2019; Whitlock and Guillaume 2009). Second, we could follow the example of Al-Asadi et al. (2019) and apply our measures of genetic dissimilarity to haplotypes of different size to estimate relative variation in the age of population structure. Third, we should test the performance of our tools under a wider range of demographic and selective scenarios to get a more nuanced picture of their strengths and weaknesses. Fourth, null models for wavelet dissimilarity could be constructed using knowledge of gene flow processes (instead of random permutation) to identify locations and scales with specific deviations from null patterns of gene flow.

4.1 Conclusion

Population genetics (like most fields) has a long history of arbitrary discretization for the purposes of mathematical, computational, and conceptual convenience. However, the real world often exists without clear boundaries between populations and where processes act simultaneously at multiple scales. We believe that wavelet transforms are one of a range of tools that can move population genetics into a richer but still useful characterization of the natural world.

4.2 Data availability

Code used to generate the simulations and analyses shown here are freely available at <https://github.com/jesserlasky/WaveletSpatialGenetic/>.

5 Acknowledgments

We thank Emily Josephs and Benjamin Peter and two anonymous reviewers for helpful comments. We thank Joanna Rifkin and JGI for help finding bugs in code.

789 6 Funding

790 This work was supported by NIH award R35GM138300 to JRL.

791 References

- 792 Ågren, Jon et al. (Mar. 2017). “Adaptive divergence in flowering time among
793 natural populations of *Arabidopsis thaliana*: Estimates of selection and QTL
794 mapping”. In: *Evolution* 71.3, pp. 550–564. ISSN: 0014-3820. DOI: 10.1111/
795 evo.13126. URL: <https://doi.org/10.1111/evo.13126> (visited on
796 08/28/2023).
- 797 Alonso-Blanco, Carlos et al. (2016). “1,135 Genomes Reveal the Global Pattern
798 of Polymorphism in *Arabidopsis thaliana*”. In: *Cell* 166, pp. 481–491. ISSN:
799 0092-8674. DOI: 10.1016/j.cell.2016.05.063.
- 800 Al-Asadi, Hussein et al. (Jan. 2019). “Estimating recent migration and
801 population-size surfaces”. en. In: *PLOS Genetics* 15.1. Publisher: Public Li-
802 brary of Science, e1007908. ISSN: 1553-7404. DOI: 10.1371/journal.pgen.
803 1007908. URL: <https://journals.plos.org/plosgenetics/article?id=10.1371/journal.pgen.1007908> (visited on 02/24/2022).
- 804 Ayton, Peter and Ilan Fischer (Dec. 2004). “The hot hand fallacy and the gam-
805 bler’s fallacy: Two faces of subjective randomness?” en. In: *Memory & Cog-
806 nition* 32.8, pp. 1369–1378. ISSN: 1532-5946. DOI: 10.3758/BF03206327.
807 URL: <https://doi.org/10.3758/BF03206327> (visited on 01/18/2024).
- 808 Barton, Nick H., Frantz Depaulis, and Alison M. Etheridge (Feb. 2002). “Neu-
809 tral Evolution in Spatially Continuous Populations”. In: *Theoretical Popu-
810 lation Biology* 61.1, pp. 31–48. ISSN: 0040-5809. DOI: 10.1006/tpbi.2001.
811 1557. URL: <https://www.sciencedirect.com/science/article/pii/S0040580901915576> (visited on 01/21/2024).
- 812 Battey, C J, Peter L Ralph, and Andrew D Kern (May 2020). “Space is the
813 Place: Effects of Continuous Spatial Structure on Analysis of Population
814 Genetic Data”. In: *Genetics* 215.1, pp. 193–214. ISSN: 1943-2631. DOI: 10.
815 1534/genetics.120.303143. URL: <https://doi.org/10.1534/genetics.120.303143> (visited on 01/28/2024).
- 816 — (June 2020). “Predicting geographic location from genetic variation with
817 deep neural networks”. In: *eLife* 9. Ed. by Patricia J Wittkopp et al. Pub-
818 lisher: eLife Sciences Publications, Ltd, e54507. ISSN: 2050-084X. DOI: 10.
819 7554/eLife.54507. URL: <https://doi.org/10.7554/eLife.54507> (vis-
820 ited on 01/25/2022).
- 821 Berg, Jeremy J. and Graham Coop (Aug. 2014). “A Population Genetic Signal
822 of Polygenic Adaptation”. In: *PLoS Genet* 10.8, e1004412. DOI: 10.1371/
823 journal.pgen.1004412. URL: <http://dx.doi.org/10.1371%2Fjournal.pgen.1004412>.
- 824 Bhatia, Gaurav et al. (Sept. 2013). “Estimating and interpreting FST: The im-
825 pact of rare variants”. en. In: *Genome Research* 23.9. Company: Cold Spring
826 Harbor Laboratory Press Distributor: Cold Spring Harbor Laboratory Press
827

- 831 Institution: Cold Spring Harbor Laboratory Press Label: Cold Spring Har-
 832 bor Laboratory Press Publisher: Cold Spring Harbor Lab, pp. 1514–1521.
 833 ISSN: 1088-9051, 1549-5469. DOI: 10.1101/gr.154831.113. URL: <http://genome.cshlp.org/content/23/9/1514> (visited on 08/06/2020).
- 834 Bishop, Anusha P., E. Anne Chambers, and Ian J. Wang (2023). “Gen-
 835 erating continuous maps of genetic diversity using moving win-
 836 dows”. en. In: *Methods in Ecology and Evolution* 14.5. _eprint:
 837 <https://besjournals.onlinelibrary.wiley.com/doi/pdf/10.1111/2041-210X.14090>, pp. 1175–1181. ISSN: 2041-210X. DOI: 10.1111/2041-210X.14090. URL: <https://onlinelibrary.wiley.com/doi/abs/10.1111/2041-210X.14090> (visited on 01/29/2024).
- 838 Blakemore, S.-J. et al. (Nov. 2003). “The detection of intentional contingencies
 839 in simple animations in patients with delusions of persecution”. en. In: *Psy-
 840 chological Medicine* 33.8. Publisher: Cambridge University Press, pp. 1433–
 841 1441. ISSN: 1469-8978, 0033-2917. DOI: 10.1017/S0033291703008341.
 842 URL: <https://www.cambridge.org/core/journals/psychological-medicine/article/detection-of-intentional-contingencies-in-simple-animations-in-patients-with-delusions-of-persecution/EB6864B67E97778980DBB47A91279AB6> (visited on 01/18/2024).
- 843 Bradburd, Gideon S., Graham M. Coop, and Peter L. Ralph (Sept. 2018).
 844 “Inferring Continuous and Discrete Population Genetic Structure Across
 845 Space”. eng. In: *Genetics* 210.1, pp. 33–52. ISSN: 1943-2631. DOI: 10.1534/genetics.118.301333.
- 846 Bradburd, Gideon S. and Peter L. Ralph (2019). “Spatial Population Genetics:
 847 It’s About Time”. In: *Annual Review of Ecology, Evolution, and System-
 848 atics* 50.1. _eprint: <https://doi.org/10.1146/annurev-ecolsys-110316-022659>,
 849 pp. 427–449. DOI: 10.1146/annurev-ecolsys-110316-022659. URL:
 850 <https://doi.org/10.1146/annurev-ecolsys-110316-022659> (visited on
 851 01/25/2024).
- 852 Castric, Vincent and Louis Bernatchez (Mar. 2003). “The rise and fall of iso-
 853 lation by distance in the anadromous brook charr (*Salvelinus fontinalis*
 854 Mitchill).” In: *Genetics* 163.3, pp. 983–996. ISSN: 0016-6731. URL: <https://www.ncbi.nlm.nih.gov/pmc/articles/PMC1462472/> (visited on
 855 11/28/2022).
- 856 Cavalli-Sforza, L. L. (Mar. 1966). “Population structure and human evolution”.
 857 In: *Proceedings of the Royal Society of London. Series B. Biological Sciences*
 858 164.995. Publisher: Royal Society, pp. 362–379. DOI: 10.1098/rspb.1966.
 859 0038. URL: <http://royalsocietypublishing.org/doi/10.1098/rspb.1966.0038> (visited on 02/10/2022).
- 860 Daubechies, Ingrid (1992). *Ten lectures on wavelets*. SIAM. ISBN: 0-89871-274-2.
- 861 Duforet-Frebourg, Nicolas et al. (Apr. 2016). “Detecting Genomic Signatures
 862 of Natural Selection with Principal Component Analysis: Application to the
 863 1000 Genomes Data”. In: *Molecular Biology and Evolution* 33.4, pp. 1082–
 864 1093. ISSN: 0737-4038. DOI: 10.1093/molbev/msv334. URL: <https://doi.org/10.1093/molbev/msv334> (visited on 02/24/2022).

- 876 Excoffier, Laurent and Nicolas Ray (July 2008). "Surfing during population
 877 expansions promotes genetic revolutions and structuration". eng. In: *Trends*
 878 in *Ecology & Evolution* 23.7, pp. 347–351. ISSN: 0169-5347. DOI: 10.1016/j.tree.2008.04.004.
- 880 Fitzpatrick, Matthew C. and Stephen R. Keller (2015). "Ecological genomics
 881 meets community-level modelling of biodiversity: mapping the genomic land-
 882 scape of current and future environmental adaptation". In: *Ecology Letters*
 883 18.1, pp. 1–16. ISSN: 1461-0248. DOI: 10.1111/ele.12376. URL: <http://dx.doi.org/10.1111/ele.12376>.
- 885 François, Olivier et al. (2016). "Controlling false discoveries in genome
 886 scans for selection". en. In: *Molecular Ecology* 25.2. eprint:
 887 <https://onlinelibrary.wiley.com/doi/pdf/10.1111/mec.13513>, pp. 454–469.
 888 ISSN: 1365-294X. DOI: 10.1111/mec.13513. URL: <http://onlinelibrary-wiley-com/doi/abs/10.1111/mec.13513> (visited on 02/11/2022).
- 890 Frantz, A. C. et al. (2009). "Using spatial Bayesian methods to deter-
 891 mine the genetic structure of a continuously distributed population:
 892 clusters or isolation by distance?" en. In: *Journal of Applied Ecol-
 893 ogy* 46.2. eprint: <https://onlinelibrary.wiley.com/doi/pdf/10.1111/j.1365-2664.2008.01606.x>, pp. 493–505. ISSN: 1365-2664. DOI: 10.1111/j.1365-2664.2008.01606.x. URL: <https://onlinelibrary.wiley.com/doi/abs/10.1111/j.1365-2664.2008.01606.x> (visited on 01/26/2024).
- 897 Fyfe, Sophie et al. (Nov. 2008). "Apophenia, theory of mind and schizotypy:
 898 Perceiving meaning and intentionality in randomness". In: *Cortex*. Special
 899 Issue on "Neuropsychology of Paranormal Experiences and Beliefs" 44.10,
 900 pp. 1316–1325. ISSN: 0010-9452. DOI: 10.1111/j.cortex.2007.07.009. URL: <https://www.sciencedirect.com/science/article/pii/S0010945208001391> (visited on 01/18/2024).
- 903 Gamba, Diana et al. (Aug. 2023). *The genomics and physiology of abiotic stress-
 904 tors associated with global elevation gradients in Arabidopsis thaliana*. en.
 905 Pages: 2022.03.22.485410 Section: New Results. DOI: 10.1101/2022.03.22.
 906 485410. URL: <https://www.biorxiv.org/content/10.1101/2022.03.22.485410v3> (visited on 12/07/2023).
- 908 Gautier, Mathieu (Dec. 2015). "Genome-Wide Scan for Adaptive Divergence
 909 and Association with Population-Specific Covariates". In: *Genetics* 201.4,
 910 pp. 1555–1579. ISSN: 0016-6731. DOI: 10.1534/genetics.115.181453. URL:
 911 <https://www.ncbi.nlm.nih.gov/pmc/articles/PMC4676524/> (visited on
 912 07/07/2021).
- 913 Goudet, Jérôme (2005). "hierfstat, a package for r to compute and test
 914 hierarchical F-statistics". en. In: *Molecular Ecology Notes* 5.1. eprint:
 915 <https://onlinelibrary.wiley.com/doi/pdf/10.1111/j.1471-8286.2004.00828.x>,
 916 pp. 184–186. ISSN: 1471-8286. DOI: 10.1111/j.1471-8286.2004.00828.x. URL:
 917 <http://onlinelibrary-wiley-com/doi/abs/10.1111/j.1471-8286.2004.00828.x> (visited on 02/10/2022).
- 919 Groh, Jeffrey and Graham Coop (May 2023). "The temporal and genomic scale
 920 of selection following hybridization". In: *bioRxiv*, p. 2023.05.25.542345. DOI:

- 921 10.1101/2023.05.25.542345. URL: <https://www.ncbi.nlm.nih.gov/pmc/articles/PMC10276902/> (visited on 01/26/2024).
- 922 Haldane, J. B. S. (Jan. 1948). "The theory of a cline". eng. In: *Journal of Genetics* 48.3, pp. 277–284. ISSN: 0022-1333. DOI: 10.1007/BF02986626.
- 923 Haller, Benjamin C. and Philipp W. Messer (2019). "SLiM 3: Forward Genetic Simulations Beyond the Wright–Fisher Model". en. In: *Molecular Biology and Evolution* 36.3, pp. 632–637. DOI: 10.1093/molbev/msy228. URL: <http://academic.oup.com/mbe/advance-article/doi/10.1093/molbev/msy228/5229931> (visited on 01/19/2019).
- 924 Hancock, Zachary B., Rachel H. Toczydlowski, and Gideon S. Bradburd (Mar. 2023). "A spatial approach to jointly estimate Wright's neighborhood size and long-term effective population size". In: *bioRxiv*, p. 2023.03.10.532094. DOI: 10.1101/2023.03.10.532094. URL: <https://www.ncbi.nlm.nih.gov/pmc/articles/PMC10029013/> (visited on 01/22/2024).
- 925 Hander, Tim et al. (Mar. 2019). "Damage on plants activates Ca²⁺-dependent metacaspases for release of immunomodulatory peptides". eng. In: *Science (New York, N.Y.)* 363.6433, eaar7486. ISSN: 1095-9203. DOI: 10.1126/science.aar7486.
- 926 Hardy, Olivier J. and Xavier Vekemans (2002). "spagedi: a versatile computer program to analyse spatial genetic structure at the individual or population levels". en. In: *Molecular Ecology Notes* 2.4. eprint: <https://onlinelibrary.wiley.com/doi/pdf/10.1046/j.1471-8286.2002.00305.x>, pp. 618–620. ISSN: 1471-8286. DOI: 10.1046/j.1471-8286.2002.00305.x. URL: <https://onlinelibrary.wiley.com/doi/abs/10.1046/j.1471-8286.2002.00305.x> (visited on 01/21/2024).
- 927 Heisenberg, W. (Mar. 1927). "Über den anschaulichen Inhalt der quantentheoretischen Kinematik und Mechanik". de. In: *Zeitschrift für Physik* 43.3. Company: Springer Distributor: Springer Institution: Springer Label: Springer Number: 3 Publisher: Springer-Verlag, pp. 172–198. DOI: 10.1007/BF01397280. URL: <https://link.springer.com/article/10.1007/BF01397280> (visited on 03/21/2022).
- 928 Horton, Matthew W et al. (2012). "Genome-wide patterns of genetic variation in worldwide *Arabidopsis thaliana* accessions from the RegMap panel". In: *Nat Genet* 44, pp. 212–216. ISSN: 1546-1718. DOI: 10.1038/ng.1042. URL: <http://dx.doi.org/10.1038/ng.1042>.
- 929 Johnson, Kim L. et al. (June 2017). "Insights into the Evolution of Hydroxyproline-Rich Glycoproteins from 1000 Plant Transcriptomes". In: *Plant Physiology* 174.2, pp. 904–921. ISSN: 0032-0889. DOI: 10.1104/pp.17.00295. URL: <https://doi.org/10.1104/pp.17.00295> (visited on 08/24/2023).
- 930 Josephs, Emily B. et al. (Mar. 2019). "Detecting Adaptive Differentiation in Structured Populations with Genomic Data and Common Gardens". en. In: *Genetics* 211.3. Publisher: Genetics Section: Investigations, pp. 989–1004. ISSN: 0016-6731, 1943-2631. DOI: 10.1534/genetics.118.301786. URL: <https://www.genetics.org/content/211/3/989> (visited on 11/18/2020).

- 966 Kawecki, Tadeusz J. and Dieter Ebert (2004). "Conceptual issues in local adap-
 967 tation". In: *Ecology Letters* 7.12, pp. 1225–1241. ISSN: 1461-0248. DOI: 10.
 968 1111/j.1461-0248.2004.00684.x. URL: <http://dx.doi.org/10.1111/j.1461-0248.2004.00684.x>.
- 970 Keeley, Annika T. H. et al. (May 2017). "Habitat suitability is a poor proxy for
 971 landscape connectivity during dispersal and mating movements". In: *Land-
 972 scape and Urban Planning* 161, pp. 90–102. ISSN: 0169-2046. DOI: 10.1016/
 973 j.landurbplan.2017.01.007. URL: <https://www.sciencedirect.com/science/article/pii/S0169204617300154> (visited on 02/01/2024).
- 975 Keitt, Timothy H. (2007). "On the quantification of local variation in biodiver-
 976 sity scaling using wavelets". In: *Scaling Biodiversity*. Publisher: Cambridge
 977 University Press, pp. 168–80.
- 978 Kimura, Motoo and James F. Crow (1963). "The Measure-
 979 ment of Effective Population Number". en. In: *Evolution* 17.3.
 980 _eprint: <https://onlinelibrary.wiley.com/doi/pdf/10.1111/j.1558-5646.1963.tb03281.x>, pp. 279–288. ISSN: 1558-5646. DOI: 10.1111/j.1558-
 981 5646.1963.tb03281.x. URL: <https://onlinelibrary.wiley.com/doi/abs/10.1111/j.1558-5646.1963.tb03281.x> (visited on 01/20/2024).
- 984 Kimura, Motoo and George H. Weiss (Apr. 1964). "The Stepping Stone Model
 985 of Population Structure and the Decrease of Genetic Correlation with Dis-
 986 tance". In: *Genetics* 49.4, pp. 561–576. ISSN: 0016-6731. URL: <https://www.ncbi.nlm.nih.gov/pmc/articles/PMC1210594/> (visited on 01/22/2024).
- 988 Kirkpatrick, Mark and N. H. Barton (July 1997). "Evolution of a Species' Range". In: *The American Naturalist* 150.1. ArticleType: research-article / Full publication date: July 1997 / Copyright © 1997 The University of Chicago Press, pp. 1–23. ISSN: 00030147. URL: <http://www.jstor.org/stable/10.1086/286054>.
- 993 Lasky, Jesse R., Emily B Josephs, and Geoffrey P Morris (Jan. 2023). "Geno-
 994 type–environment associations to reveal the molecular basis of environmental
 995 adaptation". In: *The Plant Cell* 35.1, pp. 125–138. ISSN: 1040-4651. DOI: 10.
 996 1093/plcell/koac267. URL: <https://doi.org/10.1093/plcell/koac267> (visited on 02/26/2023).
- 998 Lasky, Jesse R., DAVID L. Des Marais, et al. (2012). "Characterizing genomic
 999 variation of *Arabidopsis thaliana*: the roles of geography and climate". In:
 1000 *Molecular Ecology* 21.22, pp. 5512–5529. ISSN: 1365-294X. DOI: 10.1111/j.1365-294X.2012.05709.x. URL: <http://dx.doi.org/10.1111/j.1365-294X.2012.05709.x>.
- 1003 Lasky, Jesse R. and Timothy H. Keitt (Nov. 2013). "Reserve Size and Fragmen-
 1004 tation Alter Community Assembly, Diversity, and Dynamics." In: *The Amer-
 1005 ican Naturalist* 182.5, E142–E160. ISSN: 0003-0147. DOI: 10.1086/673205.
 1006 URL: <http://dx.doi.org/10.1086/673205> (visited on 02/22/2017).
- 1007 Le Corre, Valérie et al. (Apr. 1997). "Colonization with long-distance seed
 1008 dispersal and genetic structure of maternally inherited genes in forest
 1009 trees: a simulation study". en. In: *Genetics Research* 69.2. Publisher:
 1010 Cambridge University Press, pp. 117–125. ISSN: 1469-5073, 0016-6723.
 1011 DOI: 10.1017/S0016672397002668. URL: <https://www.cambridge.org>

- 1012 org / core / journals / genetics - research / article / colonization -
 1013 with - longdistance - seed - dispersal - and - genetic - structure - of -
 1014 maternally - inherited - genes - in - forest - trees - a - simulation - study /
 1015 FFEDD8A5B195F1C01C99261FE49B6432 (visited on 11/28/2022).
- 1016 Lewontin, R. C. and J. Krakauer (May 1973). "Distribution of gene frequency
 1017 as a test of the theory of the selective neutrality of polymorphisms". eng. In:
 1018 *Genetics* 74.1, pp. 175–195. ISSN: 0016-6731.
- 1019 — (June 1975). "Testing the Heterogeneity of F Values". In: *Genetics* 80.2,
 1020 pp. 397–398. ISSN: 0016-6731. URL: <https://www.ncbi.nlm.nih.gov/pmc/articles/PMC1213337/> (visited on 02/10/2022).
- 1022 Loiselle, Bette A. et al. (1995). "Spatial Genetic Structure of a Tropical Understory Shrub, *Psychotria officinalis* (Rubiaceae)". In: *American Journal of Botany* 82.11. Publisher: Botanical Society of America, pp. 1420–1425.
 1023 ISSN: 0002-9122. DOI: 10.2307/2445869. URL: <https://www.jstor.org/stable/2445869> (visited on 01/21/2024).
- 1027 Long, Quan et al. (Aug. 2013). "Massive genomic variation and strong selection in *Arabidopsis thaliana* lines from Sweden". en. In: *Nature Genetics* 45.8. Bandiera_abtest: a Cg_type: Nature Research Journals Number: 8 Primary_atype: Research Publisher: Nature Publishing Group Subject_term: Population genetics Subject_term_id: population-genetics, pp. 884–890. ISSN: 1546-1718. DOI: 10.1038/ng.2678. URL: <http://www-nature-com/articles/ng.2678> (visited on 01/16/2022).
- 1034 Machado, Heather E et al. (June 2021). "Broad geographic sampling reveals the shared basis and environmental correlates of seasonal adaptation in *Drosophila*". In: *eLife* 10. Ed. by Magnus Nordborg, Patricia J Wittkopp, and Magnus Nordborg. Publisher: eLife Sciences Publications, Ltd, e67577. ISSN: 2050-084X. DOI: 10.7554/eLife.67577. URL: <https://doi.org/10.7554/eLife.67577> (visited on 01/24/2022).
- 1040 Malécot, G. (1948). *Les mathématiques de l'hérédité*. fre. OCLC: 832598694.
 1041 Paris: Masson & Cie.
- 1042 Manel, Stéphanie et al. (Apr. 2003). "Landscape genetics: combining landscape ecology and population genetics". en. In: *Trends in Ecology & Evolution* 18.4, pp. 189–197. ISSN: 0169-5347. DOI: 10.1016/S0169-5347(03)00008-9. URL: <https://www.sciencedirect.com/science/article/pii/S0169534703000089> (visited on 10/16/2022).
- 1047 Martínez-Berdeja, Alejandra et al. (Feb. 2020). "Functional variants of DOG1 control seed chilling responses and variation in seasonal life-history strategies in *Arabidopsis thaliana*". en. In: *Proceedings of the National Academy of Sciences* 117.5. Publisher: National Academy of Sciences Section: Biological Sciences, pp. 2526–2534. ISSN: 0027-8424, 1091-6490. DOI: 10.1073/pnas.1912451117. URL: <https://www.pnas.org/content/117/5/2526> (visited on 08/20/2021).
- 1054 McRae, Brad H. et al. (2008). "Using Circuit Theory to Model Connectivity in Ecology, Evolution, and Conservation". en. In: *Ecology* 89.10.
 1055 _eprint: <https://esajournals.onlinelibrary.wiley.com/doi/pdf/10.1890/07-1861.1>, pp. 2712–2724. ISSN: 1939-9170. DOI: 10.1890/07-1861.1. URL:

- 1058 <https://onlinelibrary.wiley.com/doi/abs/10.1890/07-1861.1>
 1059 (visited on 08/27/2023).
- 1060 McVean, Gil (Oct. 2009). “A Genealogical Interpretation of Principal Components Analysis”. en. In: *PLOS Genetics* 5.10. Publisher: Public Library of
 1061 Science, e1000686. ISSN: 1553-7404. DOI: 10.1371/journal.pgen.1000686.
 1062 URL: <https://journals.plos.org/plosgenetics/article?id=10.1371/journal.pgen.1000686> (visited on 10/14/2022).
- 1063 Muraki, S. (June 1995). “Multiscale volume representation by a DoG wavelet”.
 1064 In: *IEEE Transactions on Visualization and Computer Graphics* 1.2. Conference Name: IEEE Transactions on Visualization and Computer Graphics,
 1065 pp. 109–116. ISSN: 1941-0506. DOI: 10.1109/2945.468408.
- 1066 Nagylaki, Thomas (Oct. 1978). “A diffusion model for geographically structured
 1067 populations”. en. In: *Journal of Mathematical Biology* 6.4, pp. 375–382. ISSN:
 1068 1432-1416. DOI: 10.1007/BF02463002. URL: <https://doi.org/10.1007/BF02463002> (visited on 01/22/2024).
- 1069 Nei, Masatoshi and Takeo Maruyama (June 1975). “Lewontin-Krakauer test for
 1070 neutral genes”. In: *Genetics* 80.2, p. 395. ISSN: 0016-6731. URL: <https://www.ncbi.nlm.nih.gov/pmc/articles/PMC1213335/> (visited on
 1071 02/10/2022).
- 1072 Peter, Benjamin M, Desislava Petkova, and John Novembre (Apr. 2020). “Geographic Landscapes Reveal How Human Genetic Diversity Aligns with Geography”. In: *Molecular Biology and Evolution* 37.4, pp. 943–951. ISSN: 0737-
 1073 4038. DOI: 10.1093/molbev/msz280. URL: <https://doi.org/10.1093/molbev/msz280> (visited on 01/09/2022).
- 1074 Peterman, William E. (2018). “ResistanceGA: An R package for the optimization
 1075 of resistance surfaces using genetic algorithms”. en. In: *Methods in Ecology and Evolution* 9.6, pp. 1638–1647. ISSN: 2041-210X. DOI: 10.1111/2041-
 1076 210X.12984. URL: <https://besjournals.onlinelibrary.wiley.com/doi/abs/10.1111/2041-210X.12984> (visited on 04/14/2019).
- 1077 Petkova, Desislava, John Novembre, and Matthew Stephens (Jan. 2016). “Visualizing spatial population structure with estimated effective migration surfaces”. en. In: *Nature Genetics* 48.1. Bandiera_abtest: a Cg_type: Nature Research Journals Number: 1 Primary_atype: Research Publisher: Nature Publishing Group Subject_term: Population genetics;Software Subject_term_id: population-genetics;software, pp. 94–100. ISSN: 1546-1718. DOI: 10.1038/ng.3464. URL: <http://www-nature-com/articles/ng.3464> (visited on 09/10/2021).
- 1078 Pisupati, Rahul et al. (Dec. 2017). “Verification of *Arabidopsis* stock collections
 1079 using SNPmatch, a tool for genotyping high-plexed samples”. In: *Scientific Data* 4, p. 170184. ISSN: 2052-4463. DOI: 10.1038/sdata.2017.184. URL:
 1080 <https://www.ncbi.nlm.nih.gov/pmc/articles/PMC5744633/> (visited on
 1081 10/01/2018).
- 1082 Price, Nicholas et al. (May 2018). “Combining population genomics and fitness
 1083 QTLs to identify the genetics of local adaptation in *Arabidopsis thaliana*”.
 1084 en. In: *Proceedings of the National Academy of Sciences* 115.19, pp. 5028–

- 1103 5033. ISSN: 0027-8424, 1091-6490. DOI: 10.1073/pnas.1719998115. URL:
 1104 <http://www.pnas.org/content/115/19/5028> (visited on 06/06/2018).
- 1105 Pugach, Irina et al. (2011). "Dating the age of admixture via wavelet trans-
 1106 form analysis of genome-wide data". en. In: *Genome Biology* 12.2. Publisher:
 1107 BMC, R19. DOI: 10.1186/gb-2011-12-2-r19. URL: <https://www.ncbi.nlm.nih.gov/pmc/articles/PMC3188801/> (visited on 01/26/2024).
- 1108 Ritland, Kermit (Apr. 1996). "Estimators for pairwise relatedness and indi-
 1109 vidual inbreeding coefficients". en. In: *Genetics Research* 67.2. Publisher:
 1110 Cambridge University Press, pp. 175–185. ISSN: 1469-5073, 0016-6723. DOI:
 1111 10.1017/S0016672300033620. URL: <https://www.cambridge.org/core/journals/genetics-research/article/estimators-for-pairwise-relatedness-and-individual-inbreeding-coefficients/9AE218BF6BF09CCCE18121AA63561CF7> (visited on 01/21/2024).
- 1112 Robertson, Alan (June 1975). "Remarks on the Lewontin-Krakauer test". In:
 1113 *Genetics* 80.2, p. 396. ISSN: 1943-2631. DOI: 10.1093/genetics/80.2.396. URL:
 1114 <https://doi.org/10.1093/genetics/80.2.396> (visited on
 1115 02/10/2022).
- 1116 Rosenberg, Noah A. et al. (Dec. 2005). "Clines, Clusters, and the Effect of
 1117 Study Design on the Inference of Human Population Structure". en. In:
 1118 *PLOS Genetics* 1.6. Publisher: Public Library of Science, e70. ISSN: 1553-
 1119 7404. DOI: 10.1371/journal.pgen.0010070. URL: <https://journals.plos.org/plosgenetics/article?id=10.1371/journal.pgen.0010070>
 1120 (visited on 01/26/2024).
- 1121 Rousset (2000). "Genetic differentiation between individu-
 1122 als". en. In: *Journal of Evolutionary Biology* 13.1. eprint:
 1123 <https://onlinelibrary.wiley.com/doi/pdf/10.1046/j.1420-9101.2000.00137.x>,
 1124 pp. 58–62. ISSN: 1420-9101. DOI: 10.1046/j.1420-9101.2000.00137.x.
 1125 URL: <https://onlinelibrary.wiley.com/doi/abs/10.1046/j.1420-9101.2000.00137.x> (visited on 01/21/2024).
- 1126 Rousset, François (Apr. 1997). "Genetic Differentiation and Estimation of Gene
 1127 Flow from F-Statistics Under Isolation by Distance". en. In: *Genetics* 145.4.
 1128 Publisher: Oxford Academic, pp. 1219–1228. DOI: 10.1093/genetics/145.
 1129 4.1219. URL: <https://dx.doi.org/10.1093/genetics/145.4.1219>
 1130 (visited on 08/27/2023).
- 1131 Saez-Aguayo, Susana et al. (Mar. 2014). "Local Evolution of Seed Flotation
 1132 in Arabidopsis". en. In: *PLOS Genetics* 10.3. Publisher: Public Library of
 1133 Science, e1004221. ISSN: 1553-7404. DOI: 10.1371/journal.pgen.1004221.
 1134 URL: <https://journals.plos.org/plosgenetics/article?id=10.1371/journal.pgen.1004221> (visited on
 1135 02/13/2022).
- 1136 Serre, David and Svante Pääbo (Sept. 2004). "Evidence for Gradients of Human
 1137 Genetic Diversity Within and Among Continents". In: *Genome Research*
 1138 14.9, pp. 1679–1685. ISSN: 1088-9051. DOI: 10.1101/gr.2529604. URL:
 1139 <https://www.ncbi.nlm.nih.gov/pmc/articles/PMC515312/> (visited on
 1140 01/26/2024).
- 1141 Shen, Wenzhong, Jiuer Liu, and Jian-Feng Li (Nov. 2019). "Type-II Metacaspases
 1142 Mediate the Processing of Plant Elicitor Peptides in Arabidopsis". In:
 1143

- 1149 *Molecular Plant* 12.11, pp. 1524–1533. ISSN: 1674-2052. DOI: 10.1016/j.jmolphys.2019.08.003. URL: <https://www.sciencedirect.com/science/article/pii/S1674205219302643> (visited on 08/28/2023).
- 1150
1151
1152 Shirk, Andrew J. and Samuel A. Cushman (2014). “Spatially-explicit estimation of Wright’s neighborhood size in continuous populations”. In: *Frontiers in Ecology and Evolution* 2. ISSN: 2296-701X. URL: <https://frontiersin.org/articles/10.3389/fevo.2014.00062> (visited on 01/22/2024).
- 1153
1154
1155
1156
1157 Slatkin, Montgomery (Oct. 1991). “Inbreeding coefficients and coalescence times”. en. In: *Genetical Research* 58.2, pp. 167–175. ISSN: 0016-6723, 1469-5073. DOI: 10.1017/S0016672300029827. URL: https://www.cambridge.org/core/product/identifier/S0016672300029827/type/journal_article (visited on 11/28/2022).
- 1158
1159
1160
1161
1162 — (1993). “Isolation by Distance in Equilibrium and Non-Equilibrium Populations”. In: *Evolution* 47.1. Publisher: [Society for the Study of Evolution, Wiley], pp. 264–279. ISSN: 0014-3820. DOI: 10.2307/2410134. URL: <http://www.jstor.org/stable/2410134> (visited on 10/16/2022).
- 1163
1164
1165
1166 Tseng, I-Chieh et al. (Sept. 2013). “Abscisic Acid- and Stress-Induced Highly Proline-Rich Glycoproteins Regulate Root Growth in Rice”. In: *Plant Physiology* 163.1, pp. 118–134. ISSN: 0032-0889. DOI: 10.1104/pp.113.217547. URL: <https://doi.org/10.1104/pp.113.217547> (visited on 08/24/2023).
- 1167
1168
1169
1170 Vekemans, X. and O. J. Hardy (2004). “New insights from fine-scale spatial genetic structure analyses in plant populations”. en. In: *Molecular Ecology* 13.4. eprint: <https://onlinelibrary.wiley.com/doi/pdf/10.1046/j.1365-294X.2004.02076.x>, pp. 921–935. ISSN: 1365-294X. DOI: 10.1046/j.1365-294X.2004.02076.x. URL: <https://onlinelibrary.wiley.com/doi/abs/10.1046/j.1365-294X.2004.02076.x> (visited on 01/20/2024).
- 1171
1172
1173
1174
1175 Wagner, Helene H., Mariana Chávez-Pesqueira, and Brenna R. Forester (2017). “Spatial detection of outlier loci with Moran eigenvector maps”. en. In: *Molecular Ecology Resources* 17.6. eprint: <https://onlinelibrary.wiley.com/doi/pdf/10.1111/1755-0998.12653>, pp. 1122–1135. ISSN: 1755-0998. DOI: 10.1111/1755-0998.12653. URL: <https://onlinelibrary.wiley.com/doi/abs/10.1111/1755-0998.12653> (visited on 01/23/2022).
- 1176
1177
1178
1179
1180 Wang, Ian J., Wesley K. Savage, and H. Bradley Shaffer (2009). “Landscape genetics and least-cost path analysis reveal unexpected dispersal routes in the California tiger salamander (*Ambystoma californiense*)”. en. In: *Molecular Ecology* 18.7. eprint: <https://onlinelibrary.wiley.com/doi/pdf/10.1111/j.1365-294X.2009.04122.x>, pp. 1365–1374. ISSN: 1365-294X. DOI: 10.1111/j.1365-294X.2009.04122.x. URL: <http://onlinelibrary-wiley-com/doi/abs/10.1111/j.1365-294X.2009.04122.x> (visited on 10/16/2022).
- 1181
1182
1183
1184
1185 Wang, Jianan et al. (Jan. 2020). “Genomic signatures of seed mass adaptation to global precipitation gradients in sorghum”. en. In: *Heredity* 124.1. Bandiera_abtest: a Cc_license_type: cc_by Cg_type: Nature Research Journals Number: 1 Primary_atype: Research Publisher: Nature Publish-
- 1186
1187
1188
1189
1190
1191
1192
1193
1194

- 1195 ing Group Subject_term: Agricultural genetics;Evolutionary biology Sub-
 1196 ject_term_id: agricultural-genetics;evolutionary-biology, pp. 108–121. ISSN:
 1197 1365-2540. DOI: 10.1038/s41437-019-0249-4. URL: <http://www-nature-com/articles/s41437-019-0249-4> (visited on 01/05/2022).
- 1198 Weir, B. S. and C. Clark Cockerham (1984). “Estimating F-Statistics for the
 1199 Analysis of Population Structure”. In: *Evolution* 38.6. Publisher: [Society
 1200 for the Study of Evolution, Wiley], pp. 1358–1370. ISSN: 0014-3820. DOI:
 1201 10.2307/2408641. URL: <https://www.jstor.org/stable/2408641> (visited
 1202 on 08/06/2020).
- 1203 Whitlock, Michael C. and Frederic Guillaume (Nov. 2009). “Testing for Spa-
 1204 tially Divergent Selection: Comparing QST to FST”. In: *Genetics* 183.3,
 1205 pp. 1055–1063. ISSN: 0016-6731. DOI: 10.1534/genetics.108.099812. URL:
 1206 <https://www.ncbi.nlm.nih.gov/pmc/articles/PMC2778959/> (visited on
 1207 08/07/2020).
- 1208 Whitlock, Michael C. and Katie E. Lotterhos (2015). “Reliable Detection of
 1209 Loci Responsible for Local Adaptation: Inference of a Null Model through
 1210 Trimming the Distribution of FST”. In: *The American Naturalist* 186.S1.
 1211 Publisher: [The University of Chicago Press, The American Society of Nat-
 1212 uralists], S24–S36. ISSN: 0003-0147. DOI: 10.1086/682949. URL: <https://www.jstor.org/stable/10.1086/682949> (visited on 08/30/2021).
- 1213 Wright, Sewall (Mar. 1931). “EVOLUTION IN MENDELIAN POPULA-
 1214 TIONS”. In: *Genetics* 16.2, pp. 97–159. ISSN: 1943-2631. DOI: 10.1093/
 1215 genetics/16.2.97. URL: <https://doi.org/10.1093/genetics/16.2.97>
 1216 (visited on 01/22/2024).
- 1217 — (Mar. 1943). “Isolation by Distance”. In: *Genetics* 28.2, pp. 114–138. ISSN:
 1218 0016-6731. URL: <https://www.ncbi.nlm.nih.gov/pmc/articles/PMC1209196/> (visited on 01/21/2024).
- 1219 — (Jan. 1946). “Isolation by Distance under Diverse Systems of Mating”. In:
 1220 *Genetics* 31.1, pp. 39–59. ISSN: 0016-6731. URL: <https://www.ncbi.nlm.nih.gov/pmc/articles/PMC1209315/> (visited on 01/21/2024).
- 1221 — (Jan. 1949). “The genetical structure of populations”. In: *Annals of Eugenics*
 1222 15.1. Publisher: John Wiley & Sons, Ltd, pp. 323–354. ISSN: 2050-1420. DOI:
 1223 10.1111/j.1469-1809.1949.tb02451.x. URL: <http://onlinelibrary-wiley-com/doi/abs/10.1111/j.1469-1809.1949.tb02451.x> (visited on
 1224 08/06/2020).
- 1225 Yang, Wen-Yun et al. (June 2012). “A model-based approach for analysis of
 1226 spatial structure in genetic data”. In: *Nat Genet* 44.6, pp. 725–731. ISSN:
 1227 1061-4036. DOI: 10.1038/ng.2285. URL: <http://dx.doi.org/10.1038/ng.2285>.
- 1228 Yeaman, Sam et al. (2016). “Convergent local adaptation to climate in distantly
 1229 related conifers”. In: *Science* 353.6306, pp. 1431–1433.
- 1230 Zheng, Xiuwen et al. (Dec. 2012). “A high-performance computing toolset for
 1231 relatedness and principal component analysis of SNP data”. en. In: *Bioinfor-
 1232 matics* 28.24. Publisher: Oxford Academic, pp. 3326–3328. ISSN: 1367-4803.
 1233 DOI: 10.1093/bioinformatics/bts606. URL: <http://academic.oup.com/bioinformatics/article/28/24/3326/245844> (visited on 04/13/2020).

1241 Zhou, Xiang and Matthew Stephens (July 2012). "Genome-wide efficient mixed-
1242 model analysis for association studies". In: *Nat Genet* 44.7, pp. 821–824.
1243 ISSN: 1061-4036. DOI: 10.1038/ng.2310. URL: <http://dx.doi.org/10.1038/ng.2310>.
1244